Stem Cell Reports
Article

ISSCR

OPEN ACCESS

CALR frameshift mutations in MPN patient-derived iPSCs accelerate maturation of megakaryocytes

Kathrin Olschok,[1,2,10] Lijuan Han,[1,2,3,10] Marcelo A.S. de Toledo,[1,2] Janik Böhnke,[4,5] Martin Graßhoff,[6] Ivan G. Costa,[6] Alexandre Theocharides,[7] Angela Maurer,[1,2] Herdit M. Schüler,[8] Eva Miriam Buhl,[9] Kristina Pannen,[1,2] Julian Baumeister,[1,2] Milena Kalmer,[1,2] Siddharth Gupta,[1,2] Peter Boor,[9] Deniz Gezer,[1,2] Tim H. Brümmendorf,[1,2] Martin Zenke,[4,5] Nicolas Chatain,[1,2,11] and Steffen Koschmieder[1,2,11,*]

[1]Department of Hematology, Oncology, Hemostaseology, and Stem Cell Transplantation, Faculty of Medicine, RWTH Aachen University, Pauwelsstraße 30, 52074 Aachen, Germany
[2]Center for Integrated Oncology Aachen Bonn Cologne Düsseldorf (CIO ABCD), Aachen, Germany
[3]Department of Oncology, The First Affiliated Hospital of Zhengzhou University, Zhengzhou, China
[4]Institute for Biomedical Engineering, Department of Cell Biology, Faculty of Medicine, RWTH Aachen University, Aachen, Germany
[5]Helmholtz Institute for Biomedical Engineering, RWTH Aachen University, Aachen, Germany
[6]Institute for Computational Genomics Joint Research Center for Computational Biomedicine, Faculty of Medicine, RWTH Aachen University, Aachen, Germany
[7]Division of Hematology, University Hospital Zurich and University of Zurich, Zurich, Switzerland
[8]Institute for Human Genetics, Faculty of Medicine, RWTH Aachen University, Aachen, Germany
[9]Institute for Pathology, Electron Microscopy Facility, Faculty of Medicine, RWTH Aachen University, Aachen, Germany
[10]These authors contributed equally
[11]Senior author
*Correspondence: skoschmieder@ukaachen.de
https://doi.org/10.1016/j.stemcr.2021.09.019

SUMMARY

Calreticulin (CALR) mutations are driver mutations in myeloproliferative neoplasms (MPNs), leading to activation of the thrombopoietin receptor and causing abnormal megakaryopoiesis. Here, we generated patient-derived *CALR*ins5- or *CALR*del52-positive induced pluripotent stem cells (iPSCs) to establish an MPN disease model for molecular and mechanistic studies. We demonstrated myeloperoxidase deficiency in granulocytic cells derived from homozygous *CALR* mutant iPSCs, rescued by repairing the mutation using CRISPR/Cas9. iPSC-derived megakaryocytes showed characteristics of primary megakaryocytes such as formation of demarcation membrane system and cytoplasmic pro-platelet protrusions. Importantly, *CALR* mutations led to enhanced megakaryopoiesis and accelerated megakaryocytic development in a thrombopoietin-independent manner. Mechanistically, our study identified differentially regulated pathways in mutated versus unmutated megakaryocytes, such as hypoxia signaling, which represents a potential target for therapeutic intervention. Altogether, we demonstrate key aspects of mutated *CALR*-driven pathogenesis dependent on its zygosity, and found novel therapeutic targets, making our model a valuable tool for clinical drug screening in MPNs.

INTRODUCTION

Myeloproliferative neoplasms (MPNs) are a group of clonal hematopoietic disorders including polycythemia vera, essential thrombocythemia (ET), and primary myelofibrosis (PMF), characterized by their excessive increase of granulomonocytic cells, erythroid cells, and/or platelets as well as different degrees of splenomegaly and bone marrow (BM) fibrosis (Campo et al., 2011). Somatic calreticulin (CALR) mutations were discovered in patients with ET and PMF and have been shown to be mutually exclusive with Janus kinase 2 (JAK2) and thrombopoietin (TPO) receptor (*MPL*) mutations (Klampfl et al., 2013; Nangalia et al., 2013). The most common types of *CALR* mutations are 52-bp deletions (del52; type 1) and 5-bp insertions (ins5; type 2), all leading to a +1 frameshift and a novel C terminus of the CALR mutant protein. Although most *CALR* mutations are heterozygous (het), homozygous (hom) mutations have been shown to be derived from a copy-neutral loss of heterozygosity of chromosome 19p (Klampfl et al., 2013; Stengel et al., 2019; Theocharides et al., 2016).

The oncogenic functions of CALR mutant proteins rely on its binding to the TPO receptor. This leads to the constitutive activation of JAK2 downstream targets such as STAT5, ERK1/2, and AKT, thus causing cellular transformation and abnormal megakaryopoiesis, a hallmark of CALR mutation-positive MPNs (Araki et al., 2016; Chachoua et al., 2016; Han et al., 2016; Kollmann et al., 2017; Marty et al., 2016). Megakaryocytes (MKs) are platelet-releasing cells, which are known to undergo different stages of maturation (Ru et al., 2015), but the impact of *CALR* mutations on megakaryocytic differentiation and function is still incompletely understood.

It has been reported that patients carrying hom *CALR*ins5 exhibit myeloperoxidase (MPO) deficiency as a result of a post-transcriptional mechanism, most likely due to defective CALR chaperone function (Nauseef et al., 1995; Theocharides et al., 2016). Additionally, a *CALR* knockin mouse model demonstrated that hom *CALR*del52

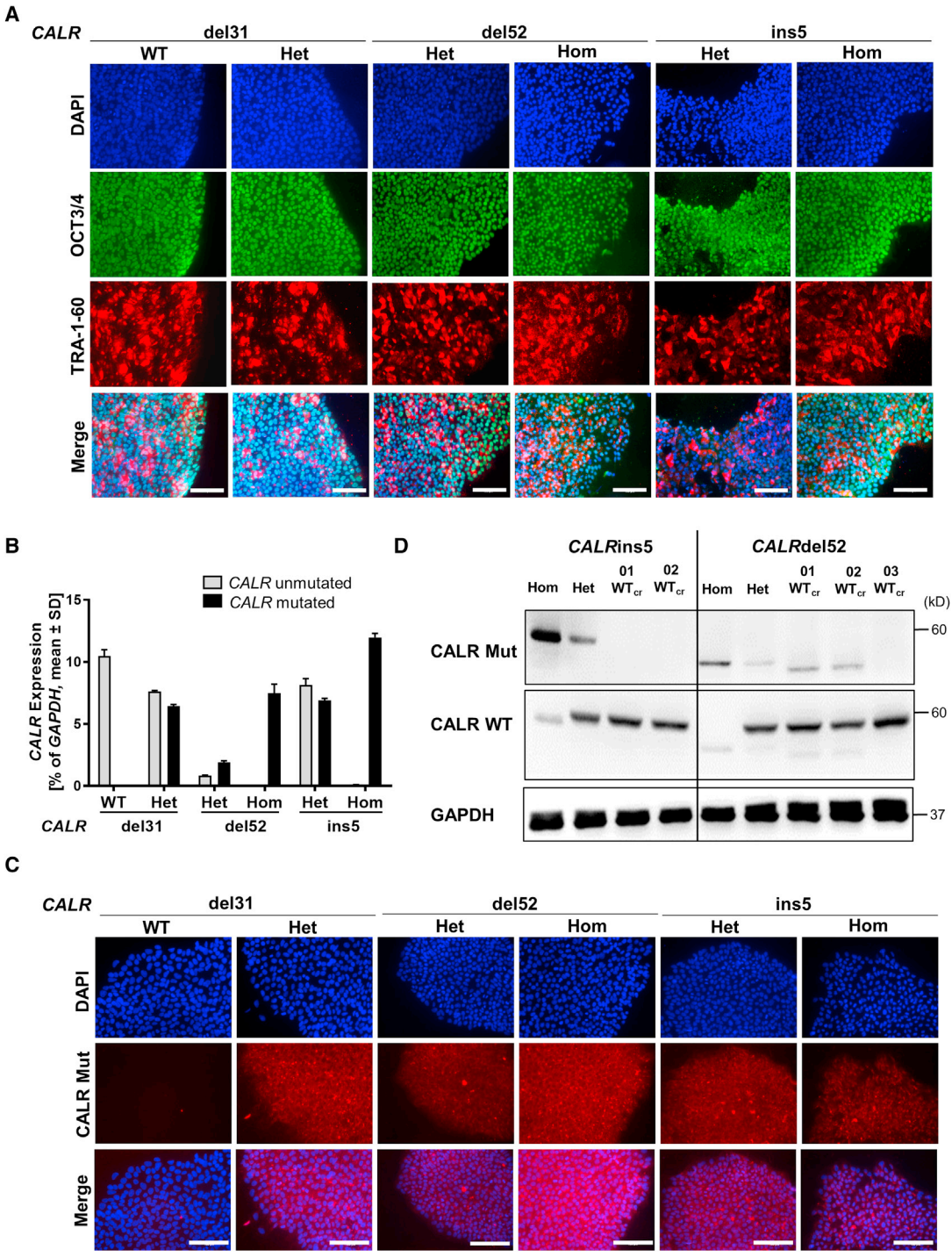

Figure 1. MPN-related iPSC clones exhibit pluripotency state and harbor *CALR* mutations

(A) Pluripotency assessment of indicated iPSC clones by immunofluorescence. Merge represents overlay of DAPI (blue), OCT3/4 (green), and TRA-1-60 (red). Scale bars, 100 μm.

(B) *CALR* mRNA expression of indicated iPSC clones was assessed by *CALR* mutant allele-specific qRT-PCR. Gene expression is depicted as percentage of *GAPDH*. Mean value ± SD of representative clones with indicated *CALR* genotypes, n = 2 independent experiments.

(legend continued on next page)

expression resulted in severe thrombocytosis and myelofibrosis (MF) phenotype (Li et al., 2018). However, the pathogenetic impact of *CALR* mutant zygosity on hematopoietic and megakaryocytic differentiation has not yet been fully addressed.

Several *CALR* mutant disease models have been used in order to uncover its molecular and cellular mechanisms in the pathogenesis of MPN. *CALR* mutant overexpressing cell line models are widely used (Araki et al., 2016; Chachoua et al., 2016; Elf et al., 2016; Han et al., 2016). However, their capacity to differentiate into hematopoietic lineages is limited. MARIMO cells, the only human cell line to date harboring mutated *CALR* (Kollmann et al., 2015), was reported to carry an additional *NRAS* Q61K mutation, which is responsible for transformation independent from mutant *CALR* (Han et al., 2018). Therefore, the validity of this cell line as a model for *CALR* mutation analysis is questionable. CALR expressing mouse models were generated showing MPN-like phenotypes *in vivo* (Benlabiod et al., 2020; Li et al., 2018; Marty et al., 2016). However, the physiological and genetic differences between species might hamper the translation of human disease phenotypes. For these reasons, *CALR* mutant MPN patient samples are desirable for analyzing biological processes. However, the clonal heterogeneity of hematopoietic stem and progenitor cell (HSPC) populations and technical limitations to isolate single clones from patients present major challenges to determining the impact of *CALR* mutant zygosity on clonal composition and diversity in MPN.

Human induced pluripotent stem cells (iPSCs) are primary cell lines with self-renewal capacity and have the potential to differentiate into any cell type of the three germ layers (Takahashi et al., 2007). Patient-derived iPSCs can be further genetically engineered with CRISPR/Cas9 technology to repair or introduce disease-related mutations in the patient's genetic background. This approach provides a valuable tool to study genotype-phenotype correlations at the clonal level.

Thus, to overcome the aforementioned limitations, we generated MPN patient-specific iPSC clones carrying hom or het *CALR* mutations or its isogenic unmutated counterpart. *CALR* mutations accelerated megakaryopoiesis independent of TPO, especially in hom mutant clones, and repair of the mutation using CRISPR/Cas9 reversed the effect. RNA sequencing (RNA-seq) of *CALR*-mutated versus non-mutated MKs demonstrated increase in hypoxia signaling and leptin expression, providing a better understanding of disease biology in ET and PMF and potential novel therapeutic targets.

RESULTS

Generation of MPN patient-derived iPSC clones and repair of hom *CALR*ins5 and *CALR*del52 mutations

iPSCs were established by reprogramming of peripheral blood mononuclear cells (PBMCs) from three MPN patients carrying *CALR*del52, *CALR*ins5, or *CALR*del31 mutations (Table S1) and two healthy donors (HDs). We obtained hom and het CALRdel52 and CALRins5 clones derived from a PMF patient and a post ET-MF patient, respectively. Additionally, het and wild-type (WT) clones were generated from a PMF patient carrying a *CALR*del31 mutation. Pluripotency of iPSCs was confirmed by positive staining for OCT3/4 and TRA-1-60 pluripotency markers (Figure 1A). Normal karyotype of MPN patient-specific iPSC clones was shown by GTG banding (Figure S1A). Expression of mutant *CALR* was confirmed by *CALR* allele-specific qRT-PCR and immunofluorescence (Figures 1B and 1C).

Reprogramming of *CALR*ins5 and *CALR*del52 PBMCs only resulted in hom and het clones but not *CALR* unmutated clones. Thus, *CALR*ins5 and *CALR*del52 mutations were repaired by CRISPR/Cas9 editing to obtain unmutated *CALR* iPSCs. Specific guide RNAs and CALR WT donor templates with homology arms were designed (Tables S2 and S3). Successful correction of *CALR* mutation in hom clones was confirmed by PCR and subsequent Sanger sequencing (Figures S1B and S1C). No off-target effects introduced by CRISPR/Cas9 were found (Figures S1D and S1E). Loss of CALR mutant protein was verified by western blotting in the CRISPR-engineered WT (WT_{cr}) clones (Figure 1D). However, clones 01 WT_{cr} and 02 WT_{cr} of the *CALR*del52 CRISPR approach showed unspecific bands when incubating with CALR-mutated antibody. To preclude that truncated versions of CALR protein resulted after the CRISPR repair, we performed standard amplification of the respective genomic region of the *CALR* gene, Sanger sequencing, and next-generation sequencing (NGS), whereby the absence of mutated genomic *CALR* sequence was confirmed (Table S4).

Using a defined NGS panel of MPN target genes (Kirschner et al., 2018), besides the *CALR* mutations no other clinically relevant MPN-related mutations were found in the generated patient-specific and HD control iPSC clones (Table S4).

(C) Mutant CALR expression (red) was confirmed by immunofluorescence staining with a CALR mutant specific antibody. Unmutated CALR iPSCs served as negative control. Nuclei were stained with DAPI (blue). Scale bars, 100 μm.

(D) Representative western blot analysis of CALR WT and CALR mutant (Mut) protein in iPSC clones after CRISPR repair of hom *CALR*ins5 and hom *CALR*del52 mutations. CALR WT protein was assessed on the same membrane as CALR mutant without stripping of the CALR Mut antibody explaining residual CALR mutant bands. GAPDH was used as loading control.

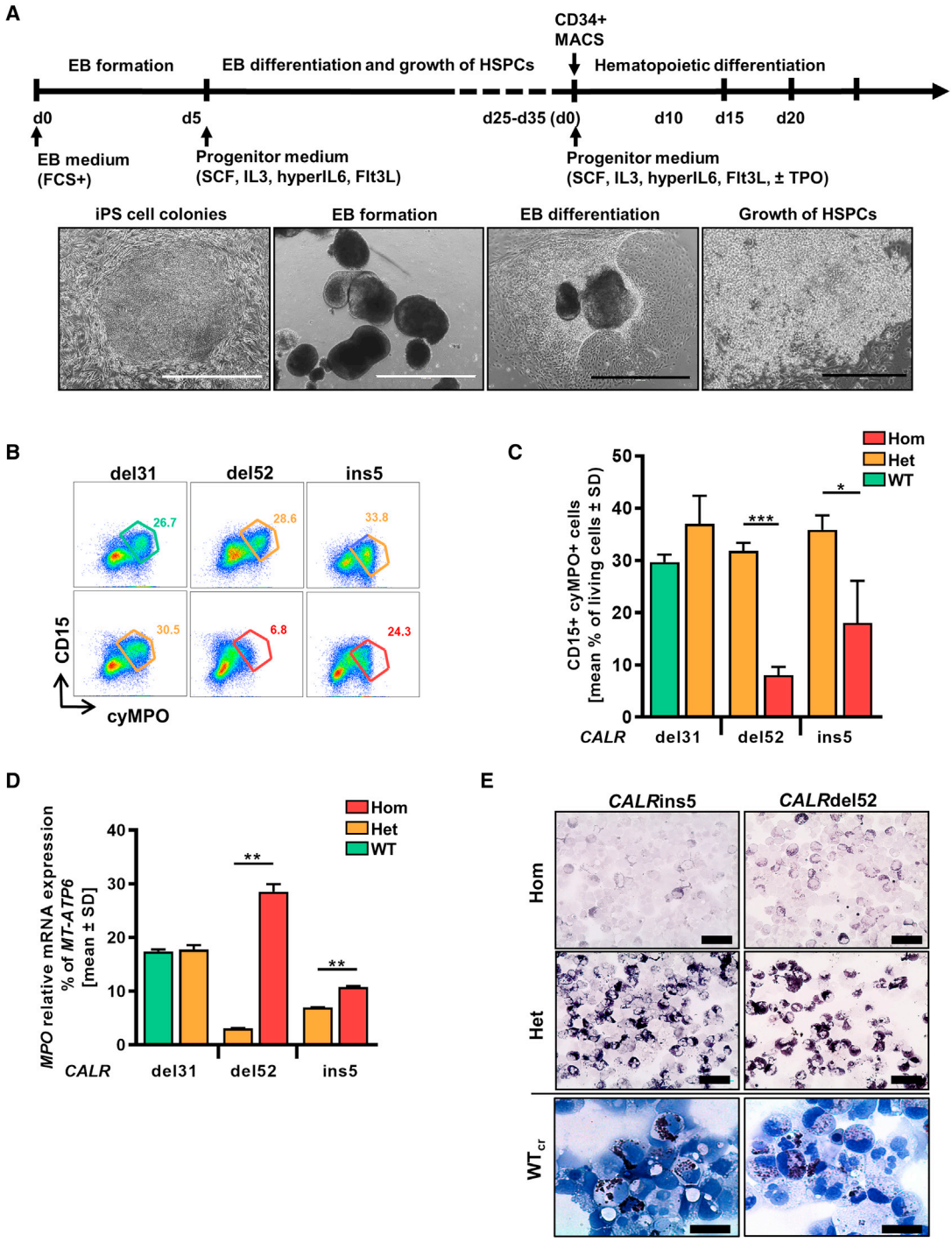

Figure 2. Restoration of MPO activity in MPN-specific iPSCs

(A) Schematic representation of an "EB-based" differentiation protocol of iPSCs toward hematopoietic progenitors. Representative images of the differentiation procedure from EB formation to HSPC production are shown. Typical morphology of iPSC colonies on day 0, embryoid bodies on day 5, mesoderm commitment and differentiated hemogenic endothelial layers on day 8, and HSPC production on day 25. Scale bars, 1,000 μm (white) and 400 μm (black).

(legend continued on next page)

MPO deficiency is detected uniquely in hom *CALR*-mutated iPSC clones and is restored in repaired *CALR* clones

Patient-derived iPSCs harboring the disease-driving mutation(s) allow disease modeling in the culture dish. Hom *CALR*ins5 lead to MPO deficiency in patients (Theocharides et al., 2016), and we recapitulated this feature *in vitro* by differentiating our iPSCs toward hematopoietic cells in a modified embryoid body (EB)-based protocol (Figure 2A) (Kovarova and Koller, 2012). We observed MPO deficiency in iPSC-derived $CD15^+$ cells harboring hom *CALR*ins5 or *CALR*del52 mutations. A significantly smaller $CD15^+cyMPO^+$ (cytoplasmic MPO) population was found in cells carrying hom *CALR*del52 and *CALR*ins5 mutations (Figures 2B and 2C). Meanwhile, relative *MPO* mRNA expression in hom *CALR* cells was upregulated (Figure 2D), confirming the post-transcriptional defect (Theocharides et al., 2016). Furthermore, a severe reduction of MPO activity in the hom *CALR*-mutated cells was confirmed by cytochemical staining (Figure 2E). Most importantly, MPO activity was rescued by the correction of hom *CALR* mutations as shown for the WT_{cr} clones, proving that the hom CALR mutation is responsible for this defect.

iPSCs harboring *CALR* mutations give rise to multiple myeloid cell lineages with stronger proliferative capacity

Next, we aimed at obtaining further mechanistical insights into CALR mutations affecting hematopoietic cells. Therefore, iPSCs that carry *CALR*del52 or *CALR*ins5 were differentiated toward the myeloid lineage with a modified differentiation protocol designated here as "spin-EB" differentiation (Figure 3A) (Liu et al., 2015). From day 8 onward, hematopoietic cells were released from the EBs into suspension, with an increase of released cells until day 14, as shown in representative images of the differentiation. Hom *CALR*ins5 and *CALR*del52 mutant clones as well as cells bearing a het *CALR*del52 mutation produced a significantly higher number of suspension cells compared with WT_{cr} cells on day 14 (Figure 3B). These data demonstrate that *CALR*ins5 and *CALR*del52 mutations enhance hematopoietic proliferation.

Flow cytometry analysis of suspension cells on days 10, 12, and 14 confirmed generation of $CD34^+CD45^+$ HSPCs (Figures S2A–S2C). To study the myeloid progenitor potential of iPSC-derived HSPCs, we performed a colony-forming unit (CFU) assay using day-14 $CD34^+$ cells, previously cultured in the presence of TPO. The het mutant *CALR*ins5 $CD34^+$ cells produced more colonies compared with WT_{cr} cells (Figure S2D). The same trend was observed for the hom *CALR*ins5 and *CALR*del52 cells compared with control ($p = 0.0898$ and $p = 0.0851$, respectively). To examine whether *CALR* mutation impacts on the expansion of $CD34^+$ cells, we evaluated the expression of the proliferative marker *Ki67* in qRT-PCR (Figure S2E). We found that HSPCs harboring a het *CALR*ins5 mutation showed higher *Ki67* expression (although not statistically significant, $p = 0.1411$) compared with WT_{cr} HSPCs. Together, these data confirmed a stronger amplification of cells in the *CALR*-mutated background, as described above. Identities of CFU-E (erythrocytic cells), CFU-M (macrophages), CFU-G (granulocytes), and CFU-GM (granulocytes/macrophages) were confirmed by morphology and Quik-Diff staining (Figure 3C). HSPCs from all analyzed clones gave rise to CFU-E, CFU-M, CFU-G, and CFU-GM colonies. While *CALR*del52 WT_{cr} HSPCs differentiated into the highest number of CFU-M, they showed less CFU-E. An increased number of erythrocytic colonies were found in het *CALR*ins5 clones.

In summary, CALR mutants accelerate hematopoietic cell proliferation, and *CALR*-mutated iPSCs show constant production of HSPCs.

CALR-mutated iPSCs exhibit enhanced TPO-independent megakaryopoiesis and accelerated maturation

Aberrant megakaryopoiesis is the major hallmark of *CALR*-mutated MPN patients as well as in established mouse models. Therefore, we studied the impact of *CALR* mutant zygosity on megakaryopoiesis in our patient-specific iPSC model in our "spin-EB" differentiation (Figure 3A) (Liu et al., 2015). We found that iPSCs carrying hom or het *CALR*ins5 and *CALR*del52 mutation gave rise to significantly more $CD41^+CD42b^+$ mature MKs compared with their WT_{cr} counterparts (Figure 4A). Moreover, no difference in

(B) Flow cytometry gating strategy to identify $cyMPO^+$ neutrophils on day 15 of "EB-based" differentiation. Exemplarily shown for iPSC-derived hematopoietic cells carrying het (orange) or hom (red) *CALR* mutation or unmutated *CALR* (green). Numbers represent frequencies of $CD15^+cyMPO^+$ populations in percentage of living single cells.

(C) Flow cytometry data for cell surface CD15 and intracellular MPO expression of iPSC-derived HSPCs on day 15 of "EB-based" differentiation. Data are shown as mean values ± SD; $^*p < 0.05$, $^{***}p < 0.001$, n = 3 independent experiments.

(D) Relative *MPO* mRNA expression was confirmed by qRT-PCR. Gene expression is depicted as percentage of *MT-ATP6*. Mean value ± SD of representative clones carrying indicated *CALR* genotypes are shown; $^{**}p < 0.01$, n = 2 independent experiments.

(E) MPO functional activity was assessed by cytochemical staining. Representative images of hematopoietic cells harboring indicated *CALR* genotypes are shown. The intensity of the black-brown dye indicates the peroxidase activity. Scale bars, 50 μm.

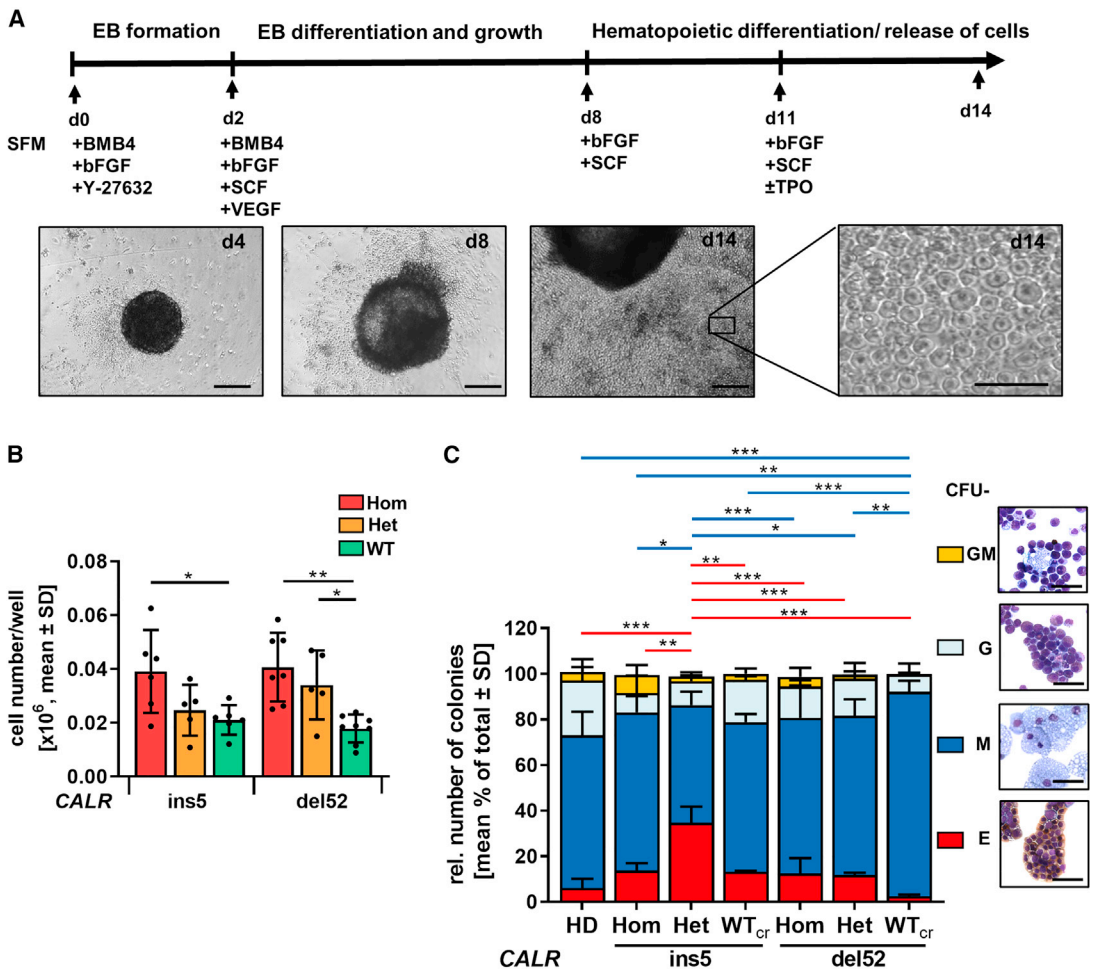

Figure 3. Hematopoietic differentiation potential of iPSC-derived CD34$^+$ cells

(A) Schematic representation of a "spin-EB" protocol to differentiate iPSCs toward hematopoietic stem cells and MKs. Cell culture medium was continuously supplemented with cytokines as indicated. On day 14, suspension cells were harvested for further analysis. Representative cell culture images of indicated days are shown. Scale bars, 50 μm.

(B) Cell number on day 14 of "spin-EB" differentiation calculated for harvested suspension cells/well of 96-well plate. Each data point represents an independent experiment for indicated *CALR* mutation and genotype shown as mean values ± SD; *p > 0.05, **p > 0.01, n = 5–8 independent differentiation experiments.

(C) Colony-forming unit (CFU) assay of purified iPSC-derived CD34$^+$ cells on day 14 of "spin-EB" differentiation. Red and blue lines refer to significant differences in CFU-E and CFU-M, respectively. Data are shown as mean values ± SD; *p > 0.05, **p > 0.01, ***p > 0.001, n = 3 independent experiments per genotype. Morphological appearance of different colony types was assessed by cytospin preparation and Diff-Quik staining. Scale bars, 50 μm.

MK numbers obtained from HD or WT_{cr} iPSCs was observed, demonstrating that the enhanced megakaryopoiesis is due to the *CALR* mutation. Mature megakaryocytes with typical multi-lobular nuclei and slight basophilic cytoplasm were detected in cytospins generated on day 14 of differentiation (Figure 4B). Of note, MKs carrying hom CALR mutation presented variable sizes, indicative of rapid maturation of aberrant MKs.

Mutant CALR binds to and activates the TPO receptor. To further study the impact of TPO on MK development in our iPSC model, we differentiated the cells with and without supplementation of TPO (Figure 4C). In HD control and WT_{cr} clones, we found a significantly lower number of MKs in the absence of TPO. In contrast, the number of iPSC-derived MKs harboring a *CALR* mutation was equal regardless of zygosity and the presence or absence of TPO. Thus, our *CALR*-mutated iPSC model recapitulates a key pathological feature of TPO-independent megakaryopoiesis.

By following *CALR*-mutated megakaryopoiesis *in vitro*, we observed a striking increase in immature CD41$^+$CD61$^+$

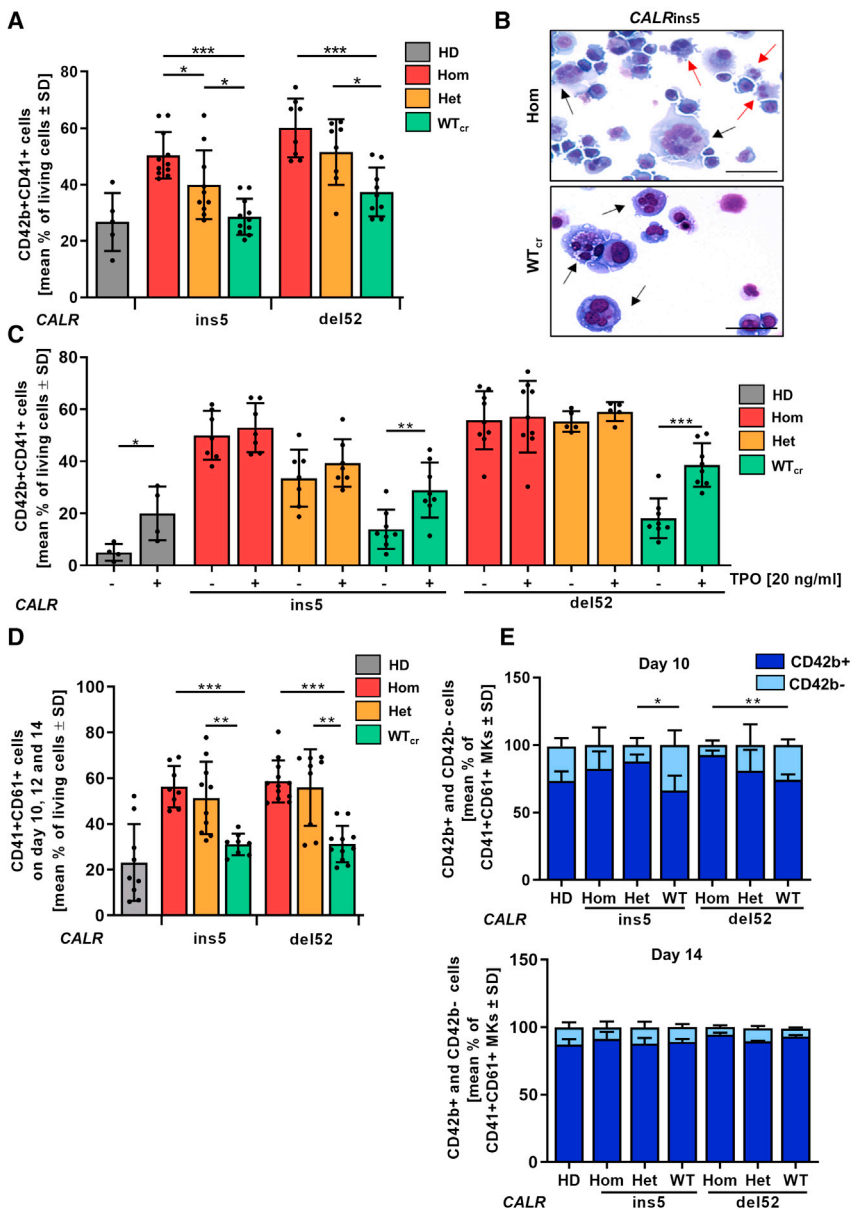

Figure 4. Megakaryocytic differentiation of *CALR*ins5 and *CALR*del52 iPSCs

(A) Percentage of $CD42b^+CD41^+$ matured MKs determined by flow cytometry on day 14 of "spin-EB" differentiation. Numbers of independent experiments performed for each *CALR* genotype and HD control refer to number of data points shown, n = 5–11 independent differentiation experiments. Data are presented as mean ± SD; *p < 0.05, **p < 0.01, ***p < 0.001.

(B) Representative morphology of MKs harvested on day 14 of "spin-EB" differentiation exemplarily shown for *CALR*ins5 hom clone and repaired WT clone (WT_{cr}) stained with Diff-Quik solutions after cytospin preparation. Typical MKs and aberrant smaller MKs are indicated by black and red arrows, respectively. Scale bars, 50 μm.

(C) Impact of TPO on MK development analyzed by flow cytometry on day 14 of "spin-EB" differentiation. Percentage of $CD42b^+CD41^+$ MKs is shown for cells treated with (+) or without (−) TPO from day 11 of differentiation onwards. Numbers of independent experiments for each *CALR* genotype and HD control refer to number of data points shown, n = 4–9 independent experiments. Data are presented as mean ± SD; *p < 0.05, **p < 0.01, ***p < 0.001.

(D) Percentage of $CD61^+CD41^+$ immature MKs determined by flow cytometry. Data of day 10, day 12, and day 14 of three independent experiments are combined for each *CALR* genotype and HD controls. Data are shown as mean values ± SD; **p < 0.01, ***p < 0.001, n = 3 independent differentiation experiments.

(E) $CD42b^+$ and $CD42b^-$ cells in $CD61^+CD41^+$ MKs on day 10 and day 14 of "spin-EB" differentiation analyzed by flow cytometry. Statistical analysis compares number of $CD42b^+$ cells of hom clones to corresponding het and WT_{cr} clones. Data are shown as mean values ± SD; **p < 0.01, n = 3 independent differentiation experiments.

MKs in comparison with unmutated cells (Figure 4D). We further analyzed the maturation kinetics in the $CD41^+CD61^+$ cell population to study differences in the MK maturity level along the differentiation, and observed less mature $CD42b^+CD41^+CD61^+$ MKs from *CALR*del52 WT_{cr} iPSCs when compared with their hom counterparts on day 10 of differentiation (Figure 4E). The same was observed for the het *CALR*ins5 clone and with a tendency (p = 0.1794) also for hom *CALR*ins5-mutated MKs. However, on day 14 all genotypes showed the same MK maturity. Altogether, these data demonstrate an accelerated MK maturation process in *CALR*-mutated cells.

MKs arise from progenitors shared with the erythrocytic lineage, the megakaryocyte-erythrocytic progenitors. Therefore, we analyzed the proportion of erythrocytic cells ($CD235a^+CD45^-$) of the day-14 population (Figure S3A). *CALR*ins5-mutated cells showed an increase in the erythrocytic population with a remarkable increase in the WT_{cr}

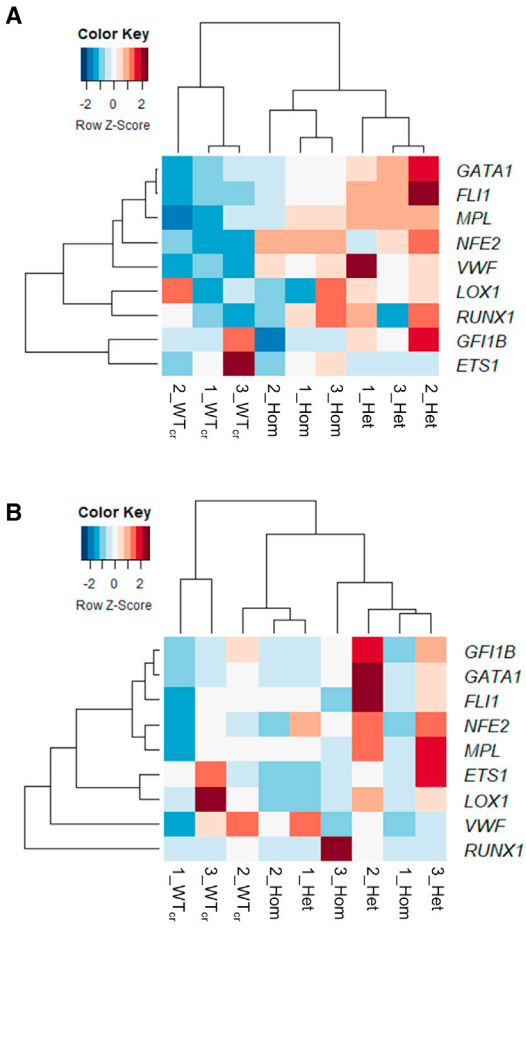

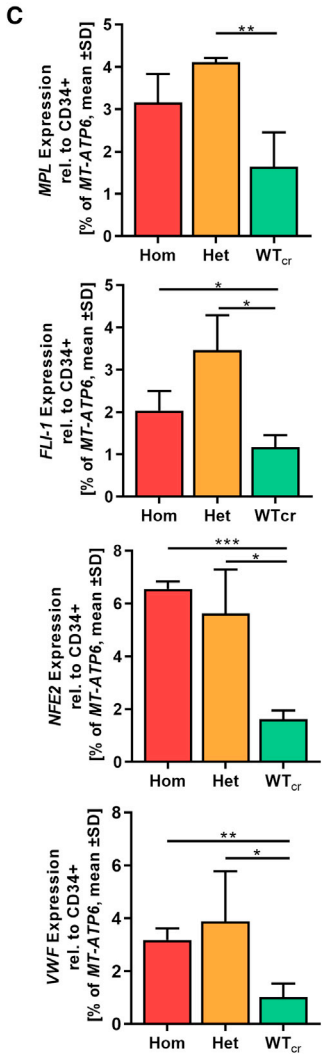

Figure 5. Gene expression profile of iPSC-derived MKs harboring *CALR* mutations

(A and B) Heatmaps for unsupervised hierarchical linkage clustering of selected MK-related genes analyzed by qRT-PCR of $CD61^+$ cells. $CD61^+$ cells were isolated by immunogenic bead selection (MACS) on day 14 of "spin-EB" differentiation. Data are normalized to gene expression of purified $CD34^+$ cells of the same experiment. Calculated *Z* score is shown for individual experiment of indicated *CALR* genotype (ins5 [A], del52 [B], with red and blue indicating high and low expression, respectively); n = 3 independent differentiation experiments for each genotype.

(C) Gene expression profile of $CD61^+$ MKs for indicated genes. Expression was normalized to $CD34^+$ cells from the same experiment. Statistical analysis compares the expression of hom and het *CALR*-mutated MKs with WT_{cr} MKs. Data are presented as mean ± SD; *p < 0.05, **p < 0.01, ***p < 0.001, n = 3 independent differentiation experiments for each genotype.

cells, different to CALRdel52 and HD control iPSCs. These data demonstrate that the repair of the *CALR* mutation in the hom *CALR*ins5-mutated cells led to enhanced erythropoiesis. Based on this, we hypothesized that differentiation properties switch upon the repair of the *CALR* mutation from the megakaryocytic to the erythrocytic lineage, at least in the patient-specific background of our *CALR*ins5-repaired clones.

CALR mutation causes upregulation of MK-related genes in iPSC-derived MKs

MK development is subjected to a highly coordinated process of MK-specific gene expression and simultaneous prevention of erythrocytic development. Our clonal approach using iPSC-derived CALR mutant MKs and their repaired counterparts are especially suitable for the analysis of solely mutated CALR-related changes. To examine whether *CALR*-mutated and -unmutated MKs show differences at the transcriptional level, we analyzed gene expression of typical megakaryocytic genes and related transcription factors.

The megakaryocytic subpopulation was purified by magnetic activated cell sorting on day 14 of "spin-EB" differentiation. We compared the differential expression signatures of MKs within the group of *CALR*ins5 MKs and *CALR*del52 MKs in a heatmap with unsupervised clustering (Figures 5A and 5B). We found that gene expression profiles (GEPs) of MKs with het or hom *CALR*ins5 mutation built a well-defined cluster compared with unmutated MKs. Of note, het *CALR*ins5-mutated MKs showed a stronger upregulation of MK-related genes compared with the hom *CALR*ins5-mutated MKs. Focusing on genes known to be

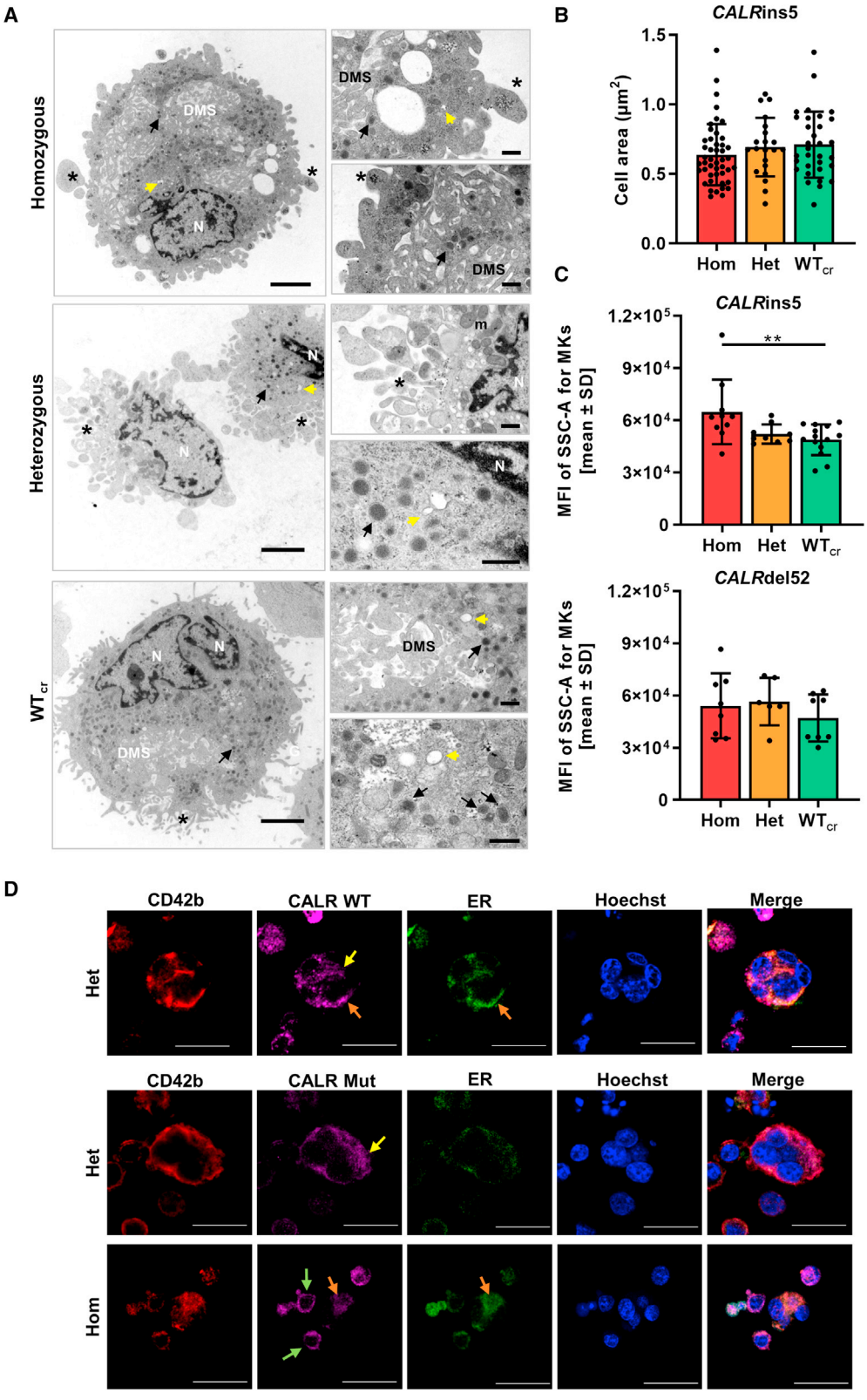

(legend on next page)

involved in megakaryocytic development, we found that the expression of MPL was slightly enhanced in *CALR*ins5 het clones and hom clones ($p = 0.0669$, Figure 5C) compared with WT_{cr} MKs. Moreover, the early transcription factor *FLI1* was highly upregulated in *CALR*ins5 het and hom MKs compared with WT_{cr} MKs ($p = 0.0106$ and $p = 0.051$, respectively). In addition, *NFE2*, an essential marker for terminal MK maturation involved in platelet release and expression of *VWF*, was strongly expressed in both hom and het *CALR*ins5-mutated MKs. Hence, hom *CALR*ins5-mutated MKs showed an upregulation of mature MK markers (*NFE2* and *VWF*), suggesting enhanced megakaryopoiesis of hom mutant cells. However, equal expression of *Ki67* in both mutated *CALR*ins5 and *CALR*del52 and unmutated MKs was observed (Figure S3B).

Unsupervised clustering of MKs with *CALR*del52 mutation did not result in clear clusters of each zygosity as given for *CALR*ins5-mutated MKs (Figure 5B). Nonetheless, gene expression of mutated MKs, both het and hom, clustered closer together than WT_{cr} MKs. In line with the expression data of *CALR*ins5-mutated MKs, the strongest upregulation of MK-related genes was found in het clones, suggesting an underlying mechanism including both mutated and WT protein, which enhances transcription of megakaryocytic genes, likely involving CALR chaperone function.

CALR-mutated MKs exhibit higher granularity

During megakaryopoiesis MKs increase in size, produce alpha and dense granules, and develop a demarcation membrane system (DMS), the plasma membrane for future platelets (Ru et al., 2015). Terminally differentiated MKs form cytoplasmic protrusions, called pro-platelets, which further mature into platelets with open canalicular systems (OCSs) (Escolar and White, 1991).

To study in more detail whether structural features of MK maturation are present in our iPSC-derived MKs, we captured ultrastructural transmission electron microscopy (TEM) images of $CD61^+$ MKs on day14 of "spin-EB" differentiation for each *CALR*ins5 genotype. TEM images of MKs with different genetic background revealed typical megakaryocytic structures including granules, DMS, pro-platelet protrusions, and OCS (Figure 6A). Additionally, we determined the area of each MK from the TEM images (Figure 6B). WT_{cr} MKs showed a slight increase ($p = 0.1679$) in size compared with hom CALR mutant MKs. This supported our previous observation that some small MKs were found in the population of hom mutant MKs in cytospin images (Figure 4B). It is reported that *in vitro* generated MKs undergo different stages of maturation, identifiable by the granularity of the cells defined by side scatter (SSC) in flow cytometry (Sim et al., 2017). Therefore, iPSC-derived $CD42b^+CD41^+CD61^+$ MKs were analyzed for their mean fluorescence intensity of SSC. We found that the granularity of MKs is significantly enhanced in the hom *CALR*ins5 MKs compared with the unmutated counterparts (Figure 6C), confirming that hom *CALR*ins5-mutated MKs showed a higher level of maturation compared with the unmutated MKs. No differences in the granularity of CALR-del52-mutated MKs was observed, again suggesting that type 1 and type 2 *CALR* mutations may not induce identical functional changes, as is also suggested by differences in their clinical profile.

In the following, we analyzed the distribution of CALR WT and mutant protein in our iPSC-derived MKs by immunofluorescence and confocal microscopy (Figures 6D and S4A). CD42b-positive MKs were identified with pronounced polylobulated nuclei in mutated and unmutated MKs, highlighted in z-stacks of hom *CALR*ins5 and WT MKs (Figure S4B). WT and mutated CALR protein were not differentially distributed in the MKs and showed a more diffuse distribution in bigger MKs (yellow arrows). However, smaller MKs with less pronounced cytoplasm showed a clustered localization of mutated CALR at the cell surface (green arrows). In some MKs, we were able to verify a co-localization of CALR protein and the ER (orange arrows).

Figure 6. Structural morphology analysis of iPSC-derived MKs and CALR distribution in MKs

(A) Transmission electron microscopy (TEM) images of iPSC-derived MKs of indicated *CALR*ins5 genotype to evaluate cell morphology. Representative images are shown. N, nucleus; DMS, demarcation membrane system; m, mitochondria. Asterisks indicate pro-platelet protrusions. Black arrows point to granules and yellow arrows indicate open canalicular system. Scale bars, 2.5 μm (large panels) and 500 nm (small panels).

(B) Calculated cell area of MKs in TEM images for indicated *CALR*ins5 genotypes. Each data point represents a single cell, n = 1 differentiation experiment. Data are presented as mean ± SD.

(C) Mean fluorescence intensity (MFI) calculated for the side scatter (SSC-A) of $CD42b^+CD41^+CD61^+$ MKs on day 14 of "spin-EB" differentiation. Indicated data points represent independent experiments for each *CALR*ins5 (n = 10–14) and *CALR*del52 (n = 6–8) genotype. Values are shown as mean ± SD; $^{**}p < 0.01$.

(D) Representative immunofluorescence images of iPSC-derived MKs stained for the ER and WT CALR or mutated (Mut) CALR after 14 days of differentiation for indicated *CALR*ins5 iPSC clones. To identify MKs, samples were additionally stained for CD42b. Hoechst was added for nuclear staining. Diffuse CALR distribution, clustered localization of CALR at the cell surface, and co-localization of CALR and ER are indicated by yellow, green, and orange arrows, respectively. Scale bars, 50 μm.

CALR mutation causes an upregulation of hypoxia-related pathways in MKs

Finally, to further unveil differences between RNA expression dependent on the zygosity of the *CALR* mutation, we performed RNA-seq analysis of day-14 CD61$^+$ iPSC-derived MKs. Three independent differentiation experiments were performed using either WT_{cr}, het, or hom *CALR*ins5-mutated iPSCs. RNA-seq data were normalized using TMM normalization (Robinson and Oshlack, 2010) and subsequently voom transformed (Law et al., 2014).

Unsupervised clustering of differentially expressed genes (DEGs) was performed and depicted in a heatmap (Figure 7A). Samples efficiently clustered according to their *CALR* mutation zygosity, and higher similarity in the GEP of mutated MKs was observed. Unsupervised subclustering of the heatmap provided cluster 1 with mainly upregulated genes and cluster 2 with downregulated DEGs in hom mutant MKs. Gene ontology (GO) analysis of those clusters showed that MKs with hom *CALR* mutation upregulated interferon signaling and the response to hypoxia, while extracellular matrix (ECM) organization was downregulated compared with WT_{cr} MKs as exemplarily shown for *FN1* (Figures 7B and S5). Of note, GO terms including genes related to the ER were found to be affected in het and hom CALR mutant MKs. The observed upregulation of hypoxia signaling was further validated by analysis of pathway responsive genes (PROGENy) (Figure 7C) (Schubert et al., 2018). Moreover, the known hypoxia-related gene *NDRG1* was significantly upregulated in both het and hom *CALR*ins5-mutated MKs compared with WT (Figure 7D). Interestingly, PROGENy analysis showed that phosphatidylinositol 3-kinase signaling was significantly downregulated in both het and hom mutant MKs compared with WT, similar to transforming growth factor β (TGFβ) and epidermal growth factor receptor pathways, which were downregulated in the hom mutant MKs compared with control MKs. In addition, a high number of DEGs was found by comparing different genotypes (Figure S6). Genes found to be significantly upregulated in both het and hom mutant MKs compared with WT_{cr} MKs included *H3C3*, *CTSF*, and leptin. Partial validation of depicted genes was performed by qRT-PCR (Figures 7D and S6D).

DISCUSSION

In the present study, we generated patient-specific iPSC lines harboring *CALR*del52, *CALR*ins5, or *CALR*del31 mutations, and the iPSC-based model was applied to study the impact of *CALR* mutant zygosity on hematopoietic and more precisely on MK differentiation at the clonal level. Patient-derived iPSCs carrying het *CALR* mutations have been recently described, but detailed comparisons of type 1 and type 2 *CALR* mutations with focus on their zygosity and detailed characterization of derived disease-driving MKs are missing (Gomez Limia et al., 2017, 2018; Secardin et al., 2021; Takei et al., 2018). To obtain isogenic *CALR*-repaired clones for *CALR*ins5 and *CALR*del52-mutated iPSCs, we used CRISPR/Cas9 technology to correct the mutations. Until now, the repair of *CALR*ins5 mutations has been reported only as a conference abstract (Wang et al., 2018), and a CRISPR/Cas9 approach has been used to model *CALR* mutations in murine cell lines (Abdelfattah and Mullally, 2018). To our knowledge, the repair of *CALR*del52 mutations in MPN-specific iPSCs has not been reported. The absence of further MPN-related mutations of clinical significance was confirmed by NGS in our *CALR*-mutated iPSC clones. Hence, our findings can be solely attributed to the *CALR* mutations.

MPO deficiency was demonstrated in hom *CALR*ins5 iPSC-derived CD15$^+$ cells and, for the first time, also in hom *CALR*del52 cells. Loss of MPO activity in MPN patients carrying hom CALR mutations was described by Theocharides et al. (2016), and we were able to restore MPO activity by CRISPR/Cas9 gene repair, demonstrating the recovery of the chaperone function of CALR. The rescue of CALR WT characteristics was underlined by the fact that WT_{cr} and HD control iPSCs generated equal levels of MKs. Importantly, the iPSC-derived MKs exhibited structural features of primary MKs such as formation of DMS, granules, multilobulated nuclei, and pro-platelets.

Megakaryocytic hyperplasia was reported for all types of MPNs and represents a diagnostic criterion of the World Health Organization (Barbui et al., 2018; Swerdlow et al., 2008; Zingariello et al., 2020). Our data demonstrate that both *CALR*ins5- and *CALR*del52-mutated iPSCs gave rise to more MKs than WT_{cr} and HD control iPSCs. In particular, hom mutant clones produced higher numbers of MKs followed by het clones. Thus, the phenotype demonstrated in our study recapitulates the phenotype found in MPN patients. Furthermore, knockin mice expressing hom *CALR*ins5 or *CALR*del52 mutations exhibited stronger ET- and PMF-related phenotypes over het CALR mutant mice, demonstrating that zygosity of the *CALR* mutation has an impact on disease development (Benlabiod et al., 2020). Araki et al. (2019) described mutant CALR protein homomultimers that are presumed to bind and activate the TPO receptor. We can assume that mutant CALR homomultimers are formed more excessively in hom clones than in het clones, since our data confirm a strong bias toward the MK lineage observed for hom *CALR*-mutated iPSCs.

Importantly, we demonstrated in our human iPSC-based model that the *CALR* mutation led to amplification of the MK lineage in a TPO-independent manner while WT and HD control cells showed pronounced MK population only in the presence of TPO. Of note, additional treatment

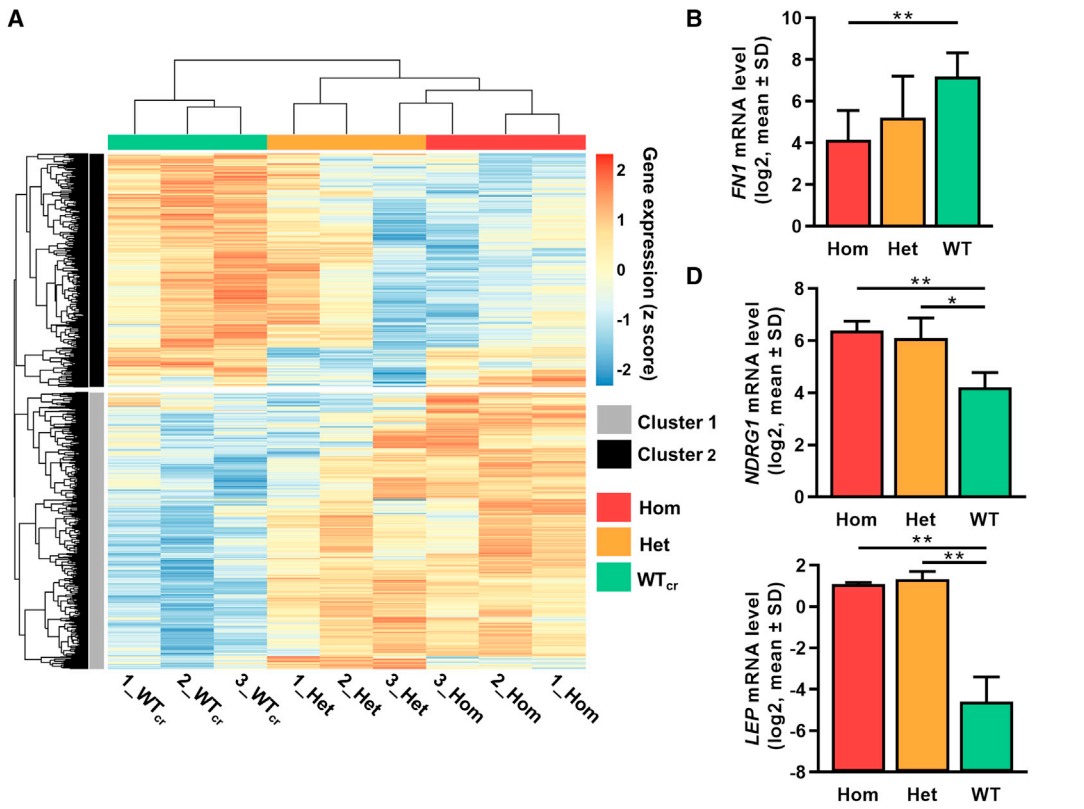

Comparison \ Pathway	Androgen	EGFR	Estrogen	Hypoxia	JAK-STAT	MAPK	NFkB	p53	PI3K	TGFb	TNFa	Trail	VEGF	WNT
Hom vs WTcr	0,154	0,021	0,435	0,012	0,194	0,114	0,435	0,662	0,021	0,021	0,277	0,561	0,951	0,277
Het vs WTcr	0,380	0,177	0,300	0,177	0,380	0,177	0,380	0,551	0,032	0,330	0,380	0,300	0,551	0,300
Hom vs Het	0,932	0,898	0,932	0,898	0,067	0,932	0,898	0,932	0,898	0,898	0,932	0,898	0,932	0,932

Figure 7. RNA-seq experiments of iPSC-derived MKs of *CALR*ins5-mutated clones

(A) Heatmap for unsupervised hierarchical clustering of RNA-seq data of iPSC-derived MKs with hom or het *CALR*ins5 mutation or WT_{cr} MKs. Numbers represent independent experiments. Unsupervised clustering was performed. n = 3 independent differentiation experiments.

(B) Gene expression profile of *FN1* in iPSC-derived MKs of RNA-seq analysis. Data are presented as mean ± SD; **p < 0.01, n = 3 independent differentiation experiments.

(C) Pathway responsive genes (PROGENy) of multiple comparisons of hom, het, and WT_{cr} iPSC-derived MKs. Upregulated and downregulated pathways are shown in red and blue, respectively. Adjusted p values from multiple comparisons are shown in the table. Significant values ($p_{adjusted}$ < 0.05) are highlighted in red, n = 3 independent differentiation experiments.

(D) Gene expression of *NDRG1* and *LEP* in iPSC-derived MKs of RNA-seq analysis. Data are shown as mean ± SD; *p < 0.05, **p < 0.01, n = 3 independent differentiation experiments.

of TPO did not further increase MK generation of *CALR*-mutated cells. This might be due to the reported oncogenic interaction of the TPO receptor and mutant CALR before reaching the cell surface (Masubuchi et al., 2020; Pecquet et al., 2019), already sufficiently occupying the TPO binding site. However, Secardin et al. (2021) observed an increase of CFU-MKs, generated from iPSC-derived CALR-mutated $CD34^+$ $CD43^+$ progenitors, in the presence of TPO. These differences may be clone dependent or may be due to differences between liquid cultures and collagen/fibrin-based medium.

We showed that hom and het *CALR* mutations induced an accelerated maturation of MKs. Surface expression of CD42b, which is a marker for megakaryocytic maturation (Sim et al., 2017), was increased on mutated MKs in comparison with WT_{cr} and HD control MKs at an early time point of differentiation. Furthermore, higher expression of *NFE2* in hom and het *CALR*ins5 MKs compared with WT_{cr} MKs was observed. Moreover, we found that hom *CALR*ins5-mutated MKs exhibited a higher level of cytoplasmic granularity compared with cells harboring unmutated or het *CALR*ins5. Taken together, our data demonstrate that *CALR* mutations cause an accelerated megakaryopoiesis in iPSC-derived MKs. In future work, our model can be used to study the relationship of accelerated and enhanced megakaryopoiesis with platelet production/release in *CALR*-mutated MKs.

We confirmed the upregulation of typical megakaryocytic genes such as *NFE2*, *FLI1*, and *VWF* in our iPSC-derived MKs by qRT-PCR and proceeded to an in-depth analysis of the global GEP by RNA-seq. In contrast to reported MPN-related transcriptome analysis using primary material (El-Khoury et al., 2020; Psaila et al., 2020), our model allows to study differences of the megakaryocytic transcriptome according to the underlying *CALR* genotype by analyzing a clonal cell population with a defined mutational background to elucidate aberrant megakaryopoiesis in MPN. Our RNA-seq data identified elevated *leptin* gene expression in *CALR*-mutated MKs. Leptin functions as a hormone and adipokine predominantly expressed by adipocytes (Cava and Matarese, 2004). In liver fibrosis, leptin promotes the proliferation and secretion of ECM molecules in myofibroblasts (activated hepatic stellate cells) via the leptin receptor (Vivoli et al., 2016). Also, in BM fibrosis, leptin receptor-positive mesenchymal stromal cells were identified to be responsible for collagen fiber generation and deposition (Decker et al., 2017). Hence, it is conceivable that MK-produced leptin may be implicated in myofibroblast formation in MPN and may contribute to the inflammatory environment in the BM niche.

Of note, the expression of ECM proteins was downregulated in *CALR*-mutated MKs compared with control. The composition of ECM in the BM is essential for MK differentiation and maturation (Noetzli et al., 2019). Synthesis of ECM components in MKs was described to be regulated via autocrine TGFβ1 signaling (Abbonante et al., 2016). Our PROGENy analysis revealed that TGFβ signaling was significantly downregulated in hom *CALR* mutant MKs, which may explain the downregulation of ECM genes.

In addition, the hypoxia signaling pathway was strongly upregulated in *CALR*-mutated versus -unmutated MKs. In solid tumors, it is well established that hypoxia represents a key feature of tumor survival and development (Thomlinson and Gray, 1955), and the BM stem cell niche represents an environment of relatively low oxygen level (Irigoyen et al., 2017). The major regulator of cellular response to hypoxia is the hypoxia-inducible factor 1 (HIF-1a) (Semenza, 2009). Importantly, HIF-1a promotes survival of *JAK2*V617F-positive cells and was discovered to be a promising therapeutic target (Baumeister et al., 2020). Moreover, elevated protein levels of HIF-1a were recently described in blast phase MPN samples, suggesting a role of HIF-1a in MPN disease progression (Marinaccio et al., 2021). Hence, our data support the notion that hypoxia-related factors may be promising targets in *CALR*-mutated MPNs.

Collectively, our study describes a comprehensive iPSC system for evaluating mutant *CALR*-induced phenotypes in MPN with a clonal genetic background, which is an invaluable new tool for clinical drug screening and development of personalized therapies. We identified accelerated megakaryopoiesis and the upregulation of leptin expression as well as hypoxia signaling pathways as potential pathogenic mechanisms in *CALR*-mutated MKs.

EXPERIMENTAL PROCEDURES

Ethics approval and consent to participate

PBMCs were obtained from MPN patients carrying *CALR*del52 or *CALR*ins5 mutation at the Department of Hematology at Zurich University, and from a *CALR*del31-mutated MPN patient at the centralized Biomaterial Bank in RWTH Aachen University Hospital. Healthy donor PBMCs were provided from the Transfusion Medicine in the University Hospital, RWTH Aachen. All PBMCs were donated after written informed consent, as approved by the ethics committees in Zurich and the Medical Faculty of RWTH Aachen (EK127/12, EK 206/09, and EK099/14).

Generation of MPN patient-specific and healthy donor iPSCs

PBMCs were reprogrammed using a CytoTune iPS 2.0 Sendai Reprogramming Kit (Thermo Fisher Scientific, Waltham, MA, USA) according to the manufacturer's instructions. After reprogramming, iPSCs were seeded as single cells and individual colonies were picked and screened for *CALR* genotypes by PCR or allele-specific PCR.

Differentiation of iPSCs into hematopoietic stem cells and myeloid subsets with the "spin-EB" protocol

Feeder-free iPSC culture was maintained on Matrigel-coated 6-well plates and routinely passaged with Accutase or 0.5 mM EDTA (both Thermo Fisher Scientific). Human iPSCs were differentiated into HSPCs, MKs, and erythrocytic cells adapted from the differentiation protocol by Liu et al. (2015). Details can be found in supplemental experimental procedures.

Statistical analysis

Graphical display and statistical analysis were performed with Prism 9 (GraphPad, San Diego, CSA, USA). In every experiment two different clones for each *CALR* genotype were used, except for the het *CALR*del52 clone. Comparisons among two groups were performed by using unpaired Student's t tests. For multiple group comparisons, ANOVA with Bonferroni post test was performed. p values of <0.05 were considered statistically significant (*$p < 0.05$, **$p < 0.01$, ***$p < 0.001$ in figures).

Additional methods

NGS, undirected hematopoietic differentiation, magnetic activated cell sorting of HSPCs and MKs, CFU assay, SDS-PAGE and western blot, CRISPR/Cas9-mediated *CALR* mutation repair, TEM, immunofluorescence staining, cytogenic analysis, flow cytometry, cell morphology analysis, MPO cytochemical staining, RNA isolation, preparation of samples for RNA-seq, and qRT-PCR including list of primers, antibodies, and media compositions are described in supplemental information.

Data availability

RNA-seq data are available at the Gene Expression Omnibus under accession number GEO: GSE182479.

SUPPLEMENTAL INFORMATION

Supplemental information can be found online at https://doi.org/10.1016/j.stemcr.2021.09.019.

AUTHOR CONTRIBUTIONS

Conceptualization, K.O., L.H., M.A.S.d.T., N.C., and S.K.; data curation, J.B., M.G., I.G.C., and A.M.; formal analysis, K.O., L.H., M.A.S.d.T., M.G., I.G.C., A.M., and J.B.; investigation, K.O., L.H., M.A.S.d.T., J.B., A.M., H.M.S., E.M.B., K.P., S.G., and P.B.; methodology, K.O., L.H., M.A.S.d.T., and J.B.; resources, A.T., M.K., D.G., and M.Z.; supervision, M.A.S.d.T., N.C., and S.K.; visualization, K.O., L.H., M.A.S.d.T., and M.G.; writing – original draft, K.O., and L.H.; writing – review & editing, K.O., L.H., M.A.S.d.T., M.G., I.G.C., A.M., M.K., P.B., T.H.B., M.Z., N.C., and S.K.

CONFLICT OF INTERESTS

S.K. reports funding from Novartis, Bristol-Myers Squibb, and Janssen/Geron; advisory board honoraria from Pfizer, Incyte, Ariad, Novartis, AOP Pharma, BMS, Celgene, Geron, Janssen, CTI, Roche, Baxalta, and Sanofi; patent for BET inhibitor at RWTH Aachen University; honoraria from Novartis, BMS, Celgene, Geron, Janssen, Pfizer, Incyte, Ariad, Shire, Roche, and AOP Pharma; and other financial support (e.g., travel support) from Alexion, Novartis, BMS, Incyte, Ariad, AOP Pharma, Baxalta, CTI, Pfizer, Sanofi, Celgene, Shire, Janssen, Geron, Abbvie, and Karthos.

ACKNOWLEDGMENTS

We thank Reinhild Herwartz, Melanie Baumann, and Lucia Vankann for technical assistance with MPO cytochemical staining and flow cytometry analysis, and Ulla Gollan for cytogenetic analysis. We thank Sabrina Ernst, Carmen Schalla, and Prof. Dr. rer. nat. Gerhard Müller-Newen for technical support with immunofluorescence staining experiments. Biomaterial samples were provided by the RWTH centralized Biomaterial Bank Aachen (RWTH cBMB, Aachen, Germany) in accordance with the regulations of the biomaterial bank and the approval of the ethics committee of the medical faculty, RWTH Aachen. This work was in part supported by the Flow Cytometry Facility and the Confocal Microscopy Facility, core facilities of the Interdisciplinary Center for Clinical Research (IZKF) Aachen within the Faculty of Medicine at RWTH Aachen University. The study was supported by the Genomics Facility, and by a grant from the Interdisciplinary Center for Clinical Research within the Faculty of Medicine at RWTH Aachen University. This work was supported in part by funds from the German Research Foundation (Deutsche Forschungsgemeinschaft; DFG) to N.C. and M.Z. (428858617), I.G.C. (428857561), and S.K. (428858786) as part of the clinical Research Unit (CRU344), a research grant from the Deutsche José Carreras Leukämie-Stiftung (DJCLS 16R/2017) to S.K., and a research grant from the German Research Foundation (KO2155/6-1) to S.K.. L.H. was supported by the National Natural Science Foundation of China (no. 82000133). M.A.S.d.T. was financed by a CAPES-Alexander von Humboldt postdoctoral fellowship (99999.001703/2014-05). P.B. was supported by the German Research Foundation (DFG Project-IDs 322900939, 454024652) and the European Research Council (Consolidator Grant AIM.imaging.CKD, no. 101001791). A.T. was supported by the Prof. Dr. Max Cloëtta Foundation. Parts of this work were generated within the PhD thesis project of K.O. and L.H.

Received: July 15, 2019
Revised: September 24, 2021
Accepted: September 27, 2021
Published: October 21, 2021

REFERENCES

Abbonante, V., Di Buduo, C.A., Gruppi, C., Malara, A., Gianelli, U., Celesti, G., Anselmo, A., Laghi, L., Vercellino, M., Visai, L., et al. (2016). Thrombopoietin/TGF-β1 loop regulates megakaryocyte extracellular matrix component synthesis. Stem Cells *34*, 1123–1133.

Abdelfattah, N.S., and Mullally, A. (2018). Using CRISPR/cas9 gene editing to investigate the oncogenic activity of mutant calreticulin in cytokine dependent hematopoietic cells. J. Vis. Exp. *2018*, 56726.

Araki, M., Yang, Y., Masubuchi, N., Hironaka, Y., Takei, H., Morishita, S., Mizukami, Y., Kan, S., Shirane, S., Edahiro, Y., et al. (2016). Activation of the thrombopoietin receptor by mutant calreticulin

in CALR-mutant myeloproliferative neoplasms. Blood *127*, 1307–1316.

Araki, M., Yang, Y., Imai, M., Mizukami, Y., Kihara, Y., Sunami, Y., Masubuchi, N., Edahiro, Y., Hironaka, Y., Osaga, S., et al. (2019). Homomultimerization of mutant calreticulin is a prerequisite for MPL binding and activation. Leukemia *33*, 122–131.

Barbui, T., Thiele, J., Gisslinger, H., Kvasnicka, H.M., Vannucchi, A.M., Guglielmelli, P., Orazi, A., and Tefferi, A. (2018). The 2016 WHO classification and diagnostic criteria for myeloproliferative neoplasms: document summary and in-depth discussion. Blood Cancer J. *8*, 15.

Baumeister, J., Chatain, N., Hubrich, A., Maié, T., Costa, I.G., Denecke, B., Han, L., Küstermann, C., Sontag, S., Seré, K., et al. (2020). Hypoxia-inducible factor 1 (HIF-1) is a new therapeutic target in JAK2V617F-positive myeloproliferative neoplasms. Leukemia *34*, 1062–1074.

Benlabiod, C., Cacemiro, M.da C., Nédélec, A., Edmond, V., Muller, D., Rameau, P., Touchard, L., Gonin, P., Constantinescu, S.N., Raslova, H., et al. (2020). Calreticulin del52 and ins5 knock-in mice recapitulate different myeloproliferative phenotypes observed in patients with MPN. Nat. Commun. *11*, 4886.

Campo, E., Swerdlow, S.H., Harris, N.L., Pileri, S., Stein, H., and Jaffe, E.S. (2011). The 2008 WHO classification of lymphoid neoplasms and beyond: evolving concepts and practical applications. Blood *117*, 5019–5032.

Cava, A. La, and Matarese, G. (2004). The weight of leptin in immunity. Nat. Rev. Immunol. *4*, 371–379.

Chachoua, I., Pecquet, C., El-Khoury, M., Nivarthi, H., Albu, R.I., Marty, C., Gryshkova, V., Defour, J.P., Vertenoeil, G., Ngo, A., et al. (2016). Thrombopoietin receptor activation by myeloproliferative neoplasm associated calreticulin mutants. Blood *127*, 1325–1335.

Decker, M., Martinez-Morentin, L., Wang, G., Lee, Y., Liu, Q., Leslie, J., and Ding, L. (2017). Leptin-receptor-expressing bone marrow stromal cells are myofibroblasts in primary myelofibrosis. Nat. Cell Biol. *19*, 677–688.

El-Khoury, M., Cabagnols, X., Mosca, M., Vertenoeil, G., Marzac, C., Favale, F., Bluteau, O., Lorre, F., Tisserand, A., Rabadan Moraes, G., et al. (2020). Different impact of calreticulin mutations on human hematopoiesis in myeloproliferative neoplasms. Oncogene *39*, 5323–5337.

Elf, S., Abdelfattah, N.S., Chen, E., Perales-Patón, J., Rosen, E.A., Ko, A., Peisker, F., Florescu, N., Giannini, S., Wolach, O., et al. (2016). Mutant calreticulin requires both its mutant C-terminus and the thrombopoietin receptor for oncogenic transformation. Cancer Discov. *6*, 368–381.

Escolar, G., and White, J.G. (1991). The platelet open canalicular system: a final common pathway. Blood Cells *17*, 467–485, discussion 486-95.

Gomez Limia, C.E., Devalle, S., Reis, M., Sochacki, J., Carneiro, M., Madeiro da Costa, R., D'Andrea, M., Padilha, T., Zalcberg, I.R., Solza, C., et al. (2017). Generation and characterization of a human induced pluripotent stem (iPS) cell line derived from an acute myeloid leukemia patient evolving from primary myelofibrosis carrying the CALR 52 bp deletion and the ASXL1 p.R693X mutation. Stem Cell Res. *24*, 16–20.

Gomez Limia, C.E., Devalle, S., Reis, M., Sochacki, J., Madeiro da Costa, R., D'Andrea, M., Padilha, T., Zalcberg, I.R., Solza, C., Daumas, A., et al. (2018). Characterization of a human induced pluripotent stem (iPS) cell line (INCABRi002-A) derived from a primary myelofibrosis patient harboring the 5-bp insertion in CALR and the p.W146X mutation in TP53. Stem Cell Res. *33*, 130–134.

Han, L., Schubert, C., Köhler, J., Schemionek, M., Isfort, S., Brümmendorf, T.H., Koschmieder, S., and Chatain, N. (2016). Calreticulin-mutant proteins induce megakaryocytic signaling to transform hematopoietic cells and undergo accelerated degradation and Golgi-mediated secretion. J. Hematol. Oncol. *9*, 45.

Han, L., Czech, J., Maurer, A., Brümmendorf, T.H., Chatain, N., and Koschmieder, S. (2018). Mutant NRAS Q61K is responsible for MAPK pathway activation in the MARIMO cell line and renders these cells independent of the CALR-MPL-JAK2-STAT5 pathway. Leukemia *32*, 2087–2090.

Irigoyen, M., García-Ruiz, J.C., and Berra, E. (2017). The hypoxia signalling pathway in haematological malignancies. Oncotarget *8*, 36832–36844.

Kirschner, M., Maurer, A., Wlodarski, M.W., Ventura Ferreira, M.S., Bouillon, A.-S., Halfmeyer, I., Blau, W., Kreuter, M., Rosewich, M., Corbacioglu, S., et al. (2018). Recurrent somatic mutations are rare in patients with cryptic dyskeratosis congenita. Leukemia *32*, 1762–1767.

Klampfl, T., Gisslinger, H., Harutyunyan, A.S., Nivarthi, H., Rumi, E., Milosevic, J.D., Them, N.C.C., Berg, T., Gisslinger, B., Pietra, D., et al. (2013). Somatic mutations of calreticulin in myeloproliferative neoplasms. N. Engl. J. Med. *369*, 2379–2390.

Kollmann, K., Nangalia, J., Warsch, W., Quentmeier, H., Bench, A., Boyd, E., Scott, M., Drexler, H.G., and Green, A.R. (2015). MARIMO cells harbor a CALR mutation but are not dependent on JAK2/STAT5 signaling. Leukemia *29*, 494–497.

Kollmann, K., Warsch, W., Gonzalez-Arias, C., Nice, F.L., Avezov, E., Milburn, J., Li, J., Dimitropoulou, D., Biddie, S., Wang, M., et al. (2017). A novel signalling screen demonstrates that CALR mutations activate essential MAPK signalling and facilitate megakaryocyte differentiation. Leukemia *31*, 934–944.

Kovarova, M., and Koller, B. (2012). Differentiation of mast cells from embryonic stem cells. Curr. Protoc. Immunol. *97*. https://doi.org/10.1002/0471142735.im22f10s97.

Law, C.W., Chen, Y., Shi, W., and Smyth, G.K. (2014). Voom: precision weights unlock linear model analysis tools for RNA-seq read counts. Genome Biol. *15*, R29. https://doi.org/10.1186/gb-2014-15-2-r29.

Li, J., Prins, D., Park, H.J., Grinfeld, J., Gonzalez-Arias, C., Loughran, S., Dovey, O.M., Klampfl, T., Bennett, C., Hamilton, T.L., et al. (2018). Mutant calreticulin knockin mice develop thrombocytosis and myelofibrosis without a stemcell self-renewal advantage. Blood *131*, 649–661.

Liu, Y., Wang, Y., Gao, Y., Forbes, J.A., Qayyum, R., Becker, L., Cheng, L., and Wang, Z.Z. (2015). Efficient generation of megakaryocytes from human induced pluripotent stem cells using food

and drug administration-approved pharmacological reagents. Stem Cells Transl. Med. *4*, 309–319.

Marinaccio, C., Suraneni, P., Celik, H., Volk, A., Wen, Q.J., Ling, T., Bulic, M., Lasho, T., Koche, R.P., Famulare, C.A., et al. (2021). LKB1/STK11 is a tumor suppressor in the progression of myeloproliferative neoplasms. Cancer Discov. *11*, 1398–1410.

Marty, C., Pecquet, C., Nivarthi, H., El-Khoury, M., Chachoua, I., Tulliez, M., Villeval, J.L., Raslova, H., Kralovics, R., Constantinescu, S.N., et al. (2016). Calreticulin mutants in mice induce an MPL-dependent thrombocytosis with frequent progression to myelofibrosis. Blood *127*, 1317–1324.

Masubuchi, N., Araki, M., Yang, Y., Hayashi, E., Imai, M., Edahiro, Y., Hironaka, Y., Mizukami, Y., Kihara, Y., Takei, H., et al. (2020). Mutant calreticulin interacts with MPL in the secretion pathway for activation on the cell surface. Leukemia *34*, 499–509.

Nangalia, J., Massie, C.E., Baxter, E.J., Nice, F.L., Gundem, G., Wedge, D.C., Avezov, E., Li, J., Kollmann, K., Kent, D.G., et al. (2013). Somatic CALR mutations in myeloproliferative neoplasms with nonmutated JAK2. N. Engl. J. Med. *369*, 2391–2405.

Nauseef, W.M., McCormick, S.J., and Clark, R.A. (1995). Calreticulin functions as a molecular chaperone in the biosynthesis of myeloperoxidase. J. Biol. Chem. *270*, 4741–4747.

Noetzli, L.J., French, S.L., and Machlus, K.R. (2019). New insights into the differentiation of megakaryocytes from hematopoietic progenitors. Arterioscler. Thromb. Vasc. Biol. *39*, 1288–1300.

Pecquet, C., Chachoua, I., Roy, A., Balligand, T., Vertenoeil, G., Leroy, E., Albu, R.I., Defour, J.P., Nivarthi, H., Hug, E., et al. (2019). Calreticulin mutants as oncogenic rogue chaperones for TpoR and traffic-defective pathogenic TpoR mutants. Blood *133*, 2669–2681.

Psaila, B., Wang, G., Rodriguez-Meira, A., Li, R., Heuston, E.F., Murphy, L., Yee, D., Hitchcock, I.S., Sousos, N., O'Sullivan, J., et al. (2020). Single-cell analyses reveal megakaryocyte-biased hematopoiesis in myelofibrosis and identify mutant clone-specific targets. Mol. Cell *78*, 477–492.e8.

Robinson, M.D., and Oshlack, A. (2010). A scaling normalization method for differential expression analysis of RNA-seq data. Genome Biol. *11*, R25.

Ru, Y.X., Zhao, S.X., Dong, S.X., Yang, Y.Q., and Eyden, B. (2015). On the maturation of megakaryocytes: a review with original observations on human in vivo cells emphasizing morphology and ultrastructure. Ultrastruct. Pathol. *39*, 79–87.

Schubert, M., Klinger, B., Klünemann, M., Sieber, A., Uhlitz, F., Sauer, S., Garnett, M.J., Blüthgen, N., and Saez-Rodriguez, J. (2018). Perturbation-response genes reveal signaling footprints in cancer gene expression. Nat. Commun. *9*, 20.

Secardin, L., Gomez Limia, C., da Silva-Benedito, S., Lordier, L., El-Khoury, M., Marty, C., Ianotto, J.-C., Raslova, H., Constantinescu, S.N., Bonamino, M.H., et al. (2021). Induced pluripotent stem cells enable disease modeling and drug screening in calreticulin del52 and ins5 myeloproliferative neoplasms. HemaSphere *5*, e593.

Semenza, G.L. (2009). Regulation of oxygen homeostasis by hypoxia-inducible factor 1. Physiology *24*, 97–106.

Sim, X., Jarocha, D., Hayes, V., Hanby, H.A., Marks, M.S., Camire, R.M., French, D.L., Poncz, M., and Gadue, P. (2017). Identifying and enriching platelet-producing human stem cell-derived megakaryocytes using factor V uptake. Blood *130*, 192–204.

Stengel, A., Jeromin, S., Haferlach, T., Meggendorfer, M., Kern, W., and Haferlach, C. (2019). Detection and characterization of homozygosity of mutated CALR by copy neutral loss of heterozygosity in myeloproliferative neoplasms among cases with high CALR mutation loads or with progressive disease. Haematologica *104*, e187–e190.

Swerdlow, S.H., Campo, E., Harris, N.L., Jaffe, E.S., Pileri, S., Stein, H., and Thiele, J. (2008). WHO Classification of Tumours of Haematopoietic and Lymphoid Tissues (WHO).

Takahashi, K., Tanabe, K., Ohnuki, M., Narita, M., Ichisaka, T., Tomoda, K., and Yamanaka, S. (2007). Induction of pluripotent stem cells from adult human fibroblasts by defined factors. Cell *131*, 861–872.

Takei, H., Edahiro, Y., Mano, S., Masubuchi, N., Mizukami, Y., Imai, M., Morishita, S., Misawa, K., Ochiai, T., Tsuneda, S., et al. (2018). Skewed megakaryopoiesis in human induced pluripotent stem cell-derived haematopoietic progenitor cells harbouring calreticulin mutations. Br. J. Haematol. *181*, 791–802.

Theocharides, A.P.A., Lundberg, P., Lakkaraju, A.K.K., Lysenko, V., Myburgh, R., Aguzzi, A., Skoda, R.C., and Manz, M.G. (2016). Homozygous calreticulin mutations in patients with myelofibrosis lead to acquired myeloperoxidase deficiency. Blood *127*, 3253–3259.

Thomlinson, R.H., and Gray, L.H. (1955). The histological structure of some human lung cancers and the possible implications for radiotherapy. Br. J. Cancer *9*, 539–549.

Vivoli, E., Di Maira, G., and Marra, F. (2016). Liver fibrosis and leptin. Curr. Pathobiol. Rep. *4*, 69–76.

Wang, W., Wang, T., Kotini, A.G., Iancu-Rubin, C., Hoffman, R., and Papapetrou, E.P. (2018). Modeling calreticulin-mutant myeloproliferative neoplasms with isogenic induced pluripotent stem cells. Blood *132*, 4319.

Zingariello, M., Rosti, V., Vannucchi, A.M., Guglielmelli, P., Mazzarini, M., Barosi, G., Genova, M.L., and Migliaccio, A.R. (2020). Shared and distinctive ultrastructural abnormalities expressed by megakaryocytes in bone marrow and spleen from patients with myelofibrosis. Front. Oncol. *10*, 584541.

Stem Cell Reports, Volume *16*

Supplemental Information

CALR frameshift mutations in MPN patient-derived iPSCs accelerate maturation of megakaryocytes

Kathrin Olschok, Lijuan Han, Marcelo A.S. de Toledo, Janik Böhnke, Martin Graßhoff, Ivan G. Costa, Alexandre Theocharides, Angela Maurer, Herdit M. Schüler, Eva Miriam Buhl, Kristina Pannen, Julian Baumeister, Milena Kalmer, Siddharth Gupta, Peter Boor, Deniz Gezer, Tim H. Brümmendorf, Martin Zenke, Nicolas Chatain, and Steffen Koschmieder

Supplemental Information

CALR frameshift mutations in MPN patient-derived iPSCs accelerate maturation of megakaryocytes

Kathrin Olschok[1,2,*], Lijuan Han[1,2,3,*], Marcelo A. S. de Toledo[1,2], Janik Böhnke[4,5], Martin Graßhoff[6], Ivan G. Costa[6] , Alexandre Theocharides[7], Angela Maurer[1,2], Herdit M. Schüler[8], Eva Miriam Buhl[9], Kristina Pannen[1,2], Julian Baumeister[1,2], Milena Kalmer[1,2], Siddharth Gupta[1,2], Peter Boor[9], Deniz Gezer[1,2], Tim H. Brümmendorf[1,2], Martin Zenke[4,5], Nicolas Chatain[1,2,#] & Steffen Koschmieder[1,2,#]

[1]Department of Hematology, Oncology, Hemostaseology, and Stem Cell Transplantation, Faculty of Medicine, RWTH Aachen University, Aachen, Germany

[2]Center for Integrated Oncology Aachen Bonn Cologne Düsseldorf (CIO ABCD)

[3]Department of Oncology, The First Affiliated Hospital of Zhengzhou University, Zhengzhou, China

[4]Institute for Biomedical Engineering, Department of Cell Biology, Faculty of Medicine, RWTH Aachen University, Aachen, Germany

[5]Helmholtz Institute for Biomedical Engineering, RWTH Aachen University, Aachen, Germany

[6]Institute for Computational Genomics Joint Research Center for Computational Biomedicine, Faculty of Medicine, RWTH Aachen University, Aachen, Germany

[7]Division of Hematology, University Hospital Zurich and University of Zurich, Zurich, Switzerland

[8]Institute for Human Genetics, Faculty of Medicine, RWTH Aachen University, Aachen, Germany

[9]Institute for Pathology, Electron Microscopy Facility, Faculty of Medicine, RWTH Aachen University, Aachen, Germany

[*]These authors contributed equally

[#]Co-senior authors

Correspondence: Prof. Dr. med. Steffen Koschmieder, Department of Hematology, Oncology, Hemostaseology, and Stem Cell Transplantation, Faculty of Medicine, RWTH Aachen University, Pauwelsstr. 30, D-52074 Aachen, Germany, Phone: +49-241-8036102; E-mail: skoschmieder@ukaachen.de

Supplemental Information

1. Supplemental Figures

Figure S1. Proof of CRISPR/Cas9 engineered *CALR* WT clones.

Figure S2. Gating strategy and impact of CALR mutations on HSPCs proliferation

Figure S3. Impact of CALR mutations on MKs proliferation capacity and on erythrocytic cell development

Figure S4. Immunofluorescence staining to determine wild type and mutant CALR distribution in the cell

Figure S5. Gene ontology (GO) analysis of *CALR*ins5-mutated iPSC-derived MKs

2. Supplemental Tables

Table S1. Generation of MPN patient-derived CALR iPSCs

Table S2. CRISPR guide RNAs (gRNAs) to repair homozygous CALR mutations with CRISPR/Cas9

Table S3. Donor template to repair homozygous CALR mutations with CRISPR/Cas9

Table S4. NGS Data of patient-derived CALR iPSCs and Healthy donor

Table S5. List of antibodies used for flow cytometry

Table S6. List of primary and secondary antibodies used for Western blot and Immunofluorescence

Table S7. List of primers used for RT-qPCR and CALR genotyping PCR

Table S8. Medium composition

3. Supplemental Experimental Procedures

-Next generation sequencing

-Cytogenetic analysis

-Immunofluorescence staining

-RNA isolation and RT-qPCR

-SDS-Page and Western blot

-Undirected hematopoietic differentiation of iPSCs into hematopoietic progenitors and myeloid subsets with the “EB-based” protocol

-Differentiation of iPSCs into hematopoietic stem cells and myeloid subsets with the “spin-EB” protocol

-Cell morphology analysis

-MPO cytochemical staining

-Flow cytometry analysis

-CRISPR/Cas9-mediated repair of homozygous *CALRins5* and *CALRdel52* mutation in iPSCs

-Purification of CD34+ HSPCs and CD61+ megakaryocytes by magnetic activated cell sorting

-Colony-forming unit assay of CD34+ HSPCs

-Transmission electron microscopy

-Preparation of samples for RNA Sequencing

1. Supplemental Figures

Figure S1.

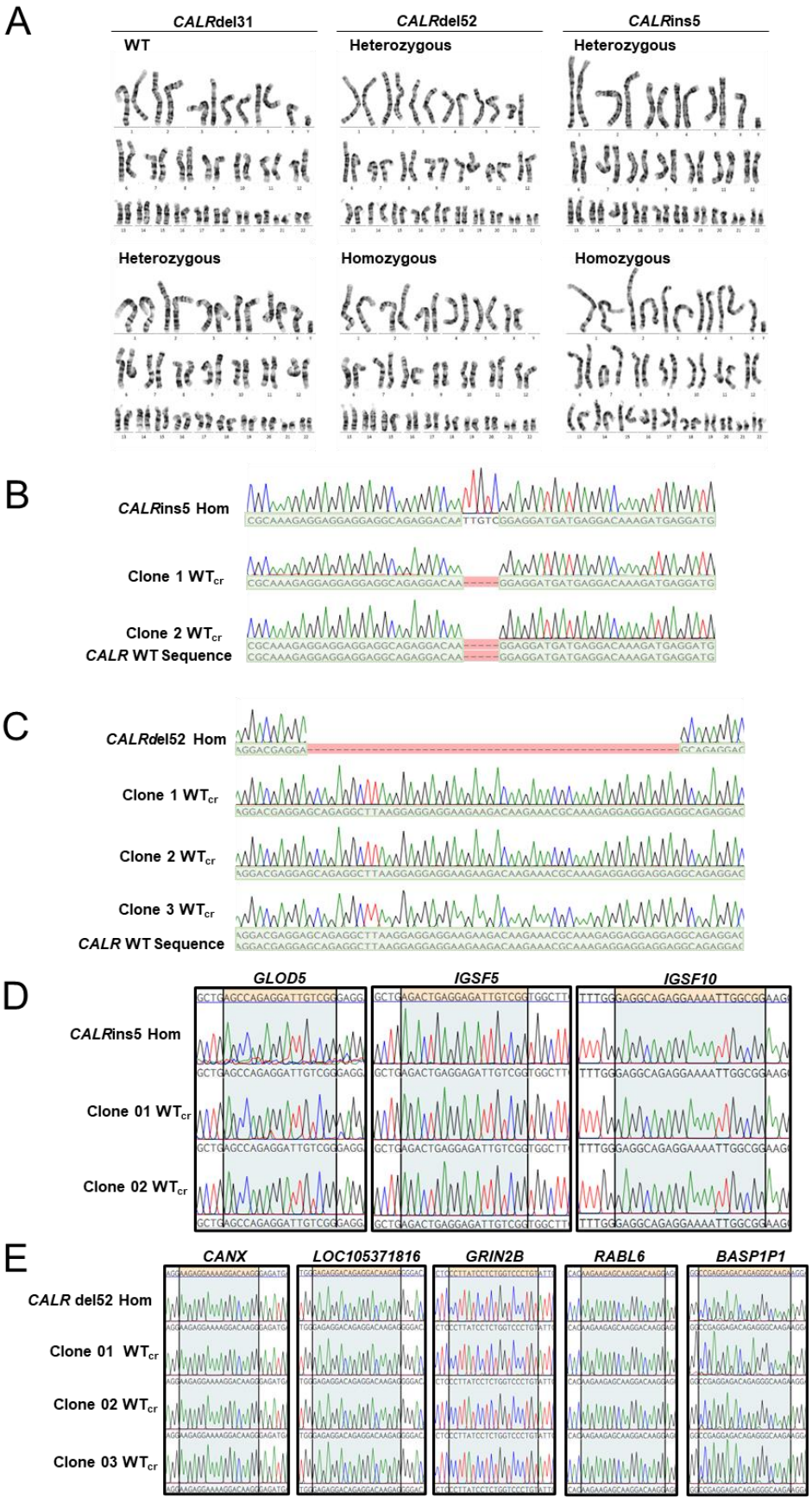

Figure S1. Proof of CRISPR/Cas9 engineered *CALR* WT clones. Related to Figure 1.

A. Karyotype analysis of patient-derived iPSC clones. **B.** Sequence alignment of maternal homozygous *CALR*ins5 clone with resulting WT_{cr} clones 01 and 02 to reference CALR WT sequence. Successful alignment and mismatch are shown in green and red, respectively. **C.** Sequence alignment of maternal homozygous *CALR*del52 clone with resulting WT_{cr} clones 01, 02, and 03 to reference CALR WT sequence. Successful alignment and mismatch are shown in green and red, respectively. **D.** and **E.** Exclusion of possible off-target effects caused by CRISPR/Cas9 gene editing for *CALR* mutations. List of off-targets was provided by IDT Systems. To verify off-target sites, regions of interest were amplified by PCR and Sanger sequenced. Sequence alignment of maternal homozygous *CALR*ins5 clone (**D**) and resulting WT_{cr} clones 01 and 02 for possible off-targets in *GLOD5*, *IGSF5,* and *IGSF10*. Regions of interest are highlighted in orange/grey. Sequence alignment of maternal homozygous *CALR*del52 clone (**E**) and resulting WT_{cr} clones 01, 02, and 03 for possible off-targets in *CANX*, *LOC105371816, GRIN2B, RABL6,* and *BASP1P1*. Regions of interest are highlighted in orange/grey.

Figure S2.

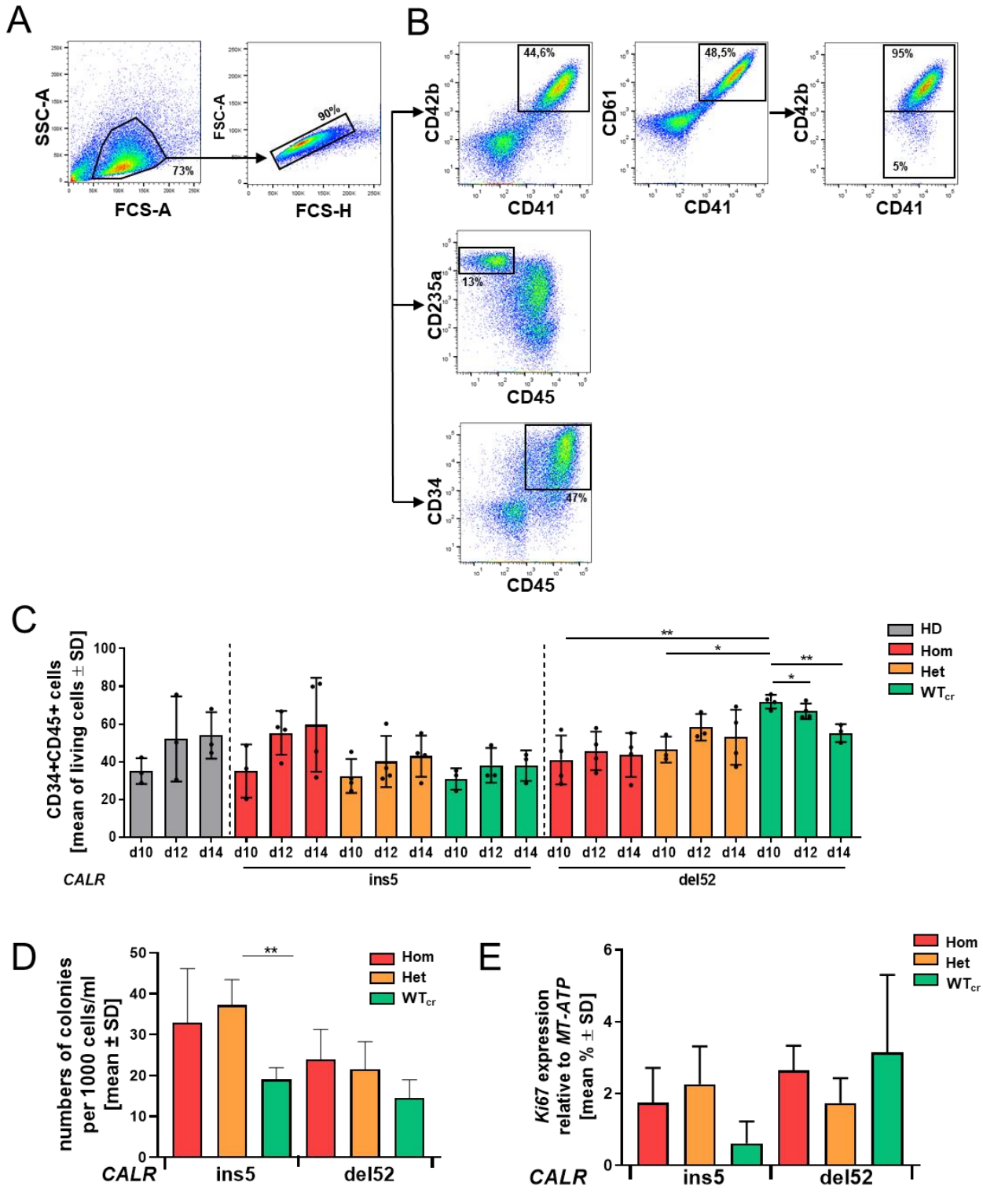
A
SSC-A
FCS-A
73%
FSC-A
FCS-H
90%
B
CD42b
CD41
44,6%
CD61
CD41
48,5%
CD42b
CD41
95%
5%
CD235a
CD45
13%
CD34
CD45
47%
C
CD34+CD45+ cells
[mean of living cells ± SD]
HD
Hom
Het
WTcr
d10 d12 d14 d10 d12 d14 d10 d12 d14 d10 d12 d14 d10 d12 d14 d10 d12 d14 d10 d12 d14
CALR
ins5
del52
D
numbers of colonies
per 1000 cells/ml
[mean ± SD]
Hom
Het
WTcr
CALR
ins5
del52
E
Ki67 expression
relative to MT-ATP
[mean % ± SD]
Hom
Het
WTcr
CALR
ins5
del52

Figure S2. Gating strategy and impact of CALR mutations on HSPCs proliferation. Related to Figure 3 and Figure 4.

A. Flow cytometry analysis gating strategy to identify myeloid cell populations in „spin-EB“ differentiation protocol. Living cells were first gated on forwards scatter (FSC-A)/side scatter (SSC-A) and further gated on single cells. **B.** Mature and immature MKs were identified by CD42b+CD41+ and CD61+CD41+, respectively. Erythroid cells were discriminated by CD235a+CD45- expression and HSPCs were determined by CD34+CD45+ expression. Numbers represent frequencies of indicated populations in percentage of living cells. **C.** Percentage of CD34+CD45+ cells on day 10, day 12 and day 14 of „spin-EB“ differentiation analyzed by flow cytometry analysis. Each data point represents an independent experiment for each *CALR* genotype and HD control shown as mean values ± SD, **p*<0.05, ***p*<0.01, *n*=3-4 independent experiments. **D.** Number of colonies counted from colony forming unit assay. Statistics was calculated by comparing mutated cells to corresponding WT_{cr} cells. Data are shown as mean values ± SD, ***p*>0.01, *n*=3-5 independent differentiation experiments. **E.** Gene expression of the proliferative marker *Ki67* measured in iPS-derived HSPC in RT-qPCR. Data are shown for three independent experiments (*n*=3) with indicated CALR genotype. Gene expression was normalized to *MT-ATP6* expression and is represented as mean values ± SD.

Figure S3.

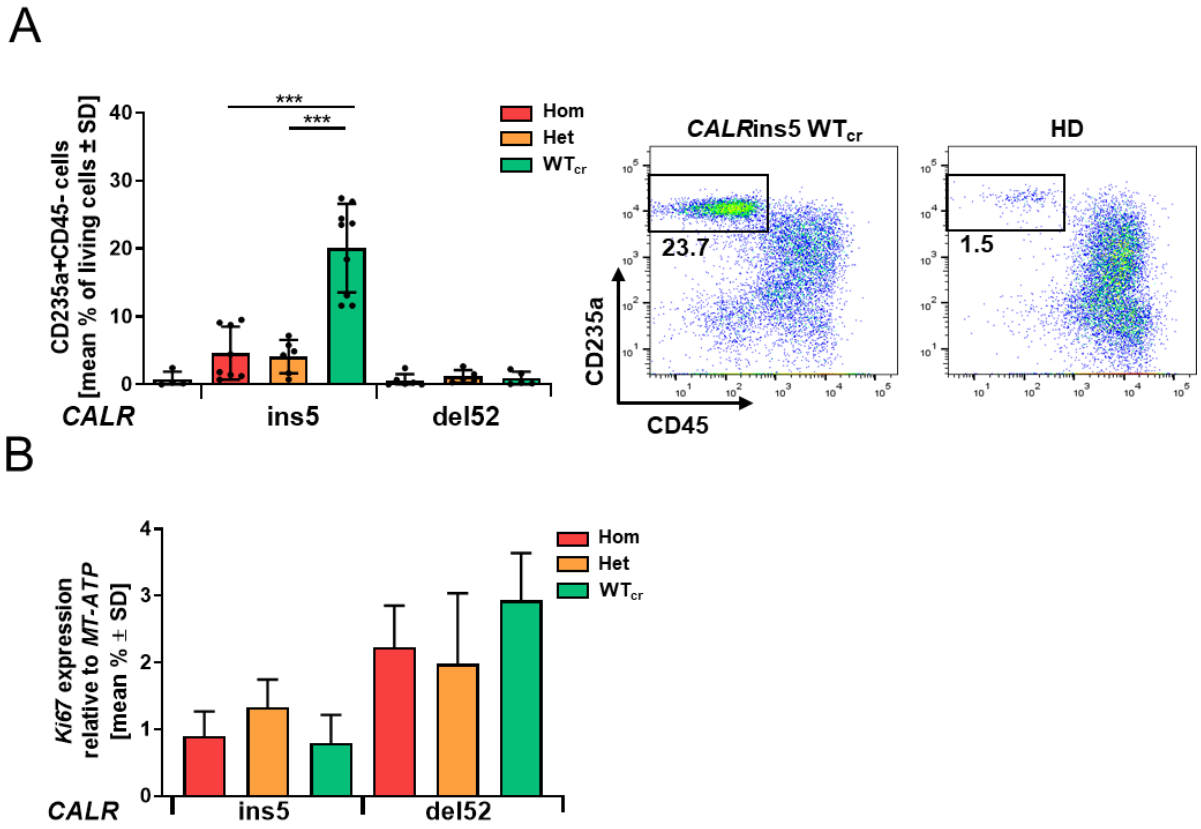

Figure S3.Impact of CALR mutations on MKs proliferation capacity and on erythrocytic cell development. Related to Figure 4.

A. Percentage of CD235a+CD45- erythroid cells determined by flow cytometry on day 14 of "spin-EB" differentiation. Number of independent experiments performed for each *CALR* genotype and HD control referred to number of data points shown, *n*=4-9. Flow cytometry plots to determine erythroid cell population (CD235a+CD45-) are exemplarily shown for *CALR*ins5 WT_{cr} cells and healthy controls. Numbers represent frequencies of indicated populations in percentage of living cells as mean values ± SD. ***p<0.001. **B.** Gene expression of the proliferative marker *Ki67* measured in iPS-derived MKs in RT-qPCR. Data are shown for three independent experiments (*n*=3) with indicated CALR genotype. Gene expression was normalized to *MT-ATP6* expression and are shown as mean values ± SD.

Figure S4.

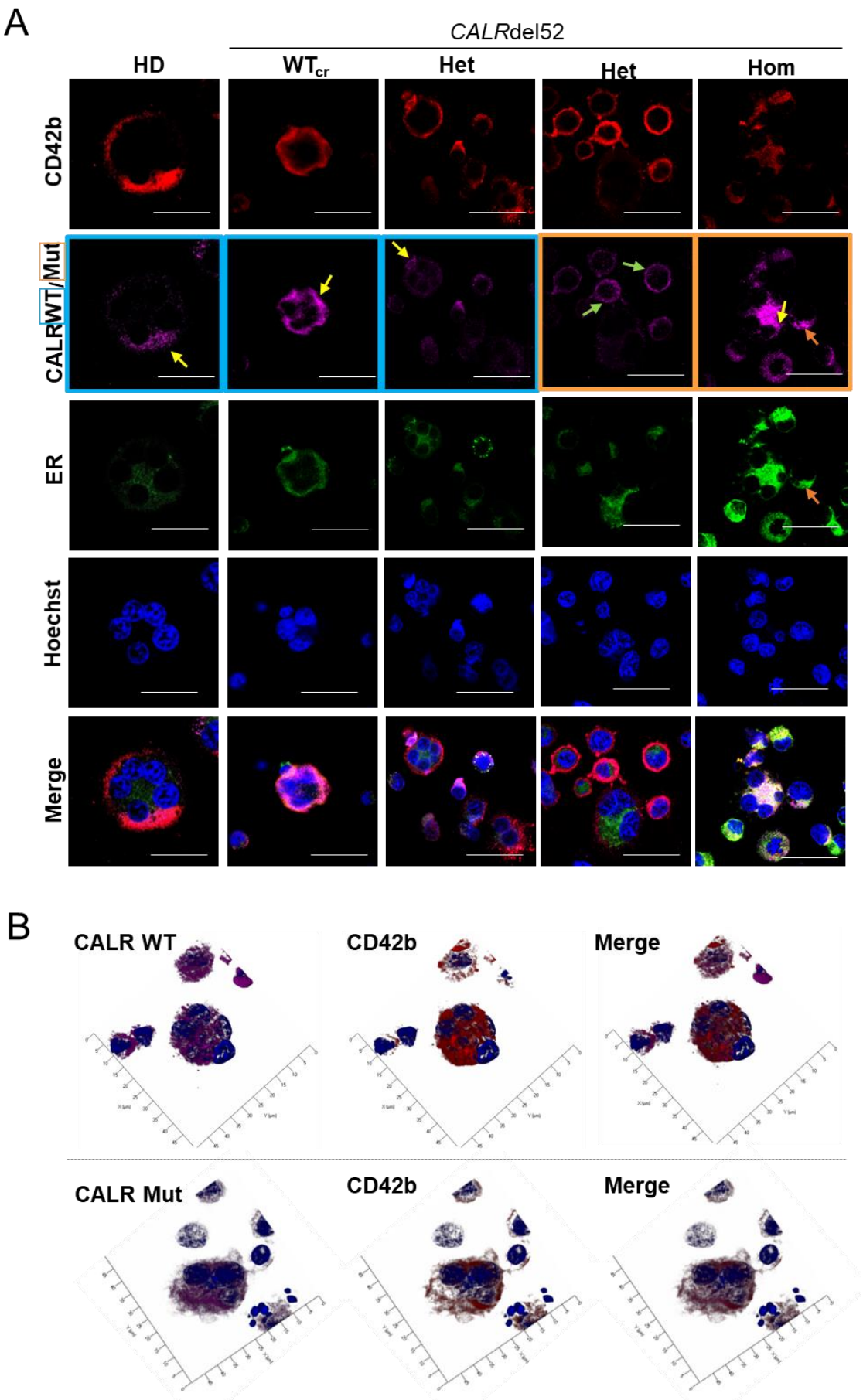
A
CALRdel52
HD
WTcr
Het
Het
Hom
CD42b
CALRWT/Mut
ER
Hoechst
Merge
B
CALR WT
CD42b
Merge
CALR Mut
CD42b
Merge

Figure S4. Immunofluorescence staining to determine wild type and mutant CALR distribution in the cell. Related to Figure 6.

A. iPSC-derived MKs were fixed and stained for the endoplasmic reticulum (ER) and wild type (WT) CALR or mutated (Mut) CALR, indicated with blue or orange frames, respectively, after 14 days of differentiation for indicated iPSC clones. To identify MKs, samples were additionally stained for CD42b. Hoechst was added for nuclear staining. Scale bars, 50 µm. Diffuse CALR distribution, clustered localization of CALR at the cell surface, and co-localization of CALR and ER are indicated with yellow, green, and orange arrows, respectively. **B.** Z-stack images of heterozygous *CALR*ins5-mutated MKs for indicated staining. Hoechst was added for nuclear staining. Scale bars, 50 µm.

Figure S5.

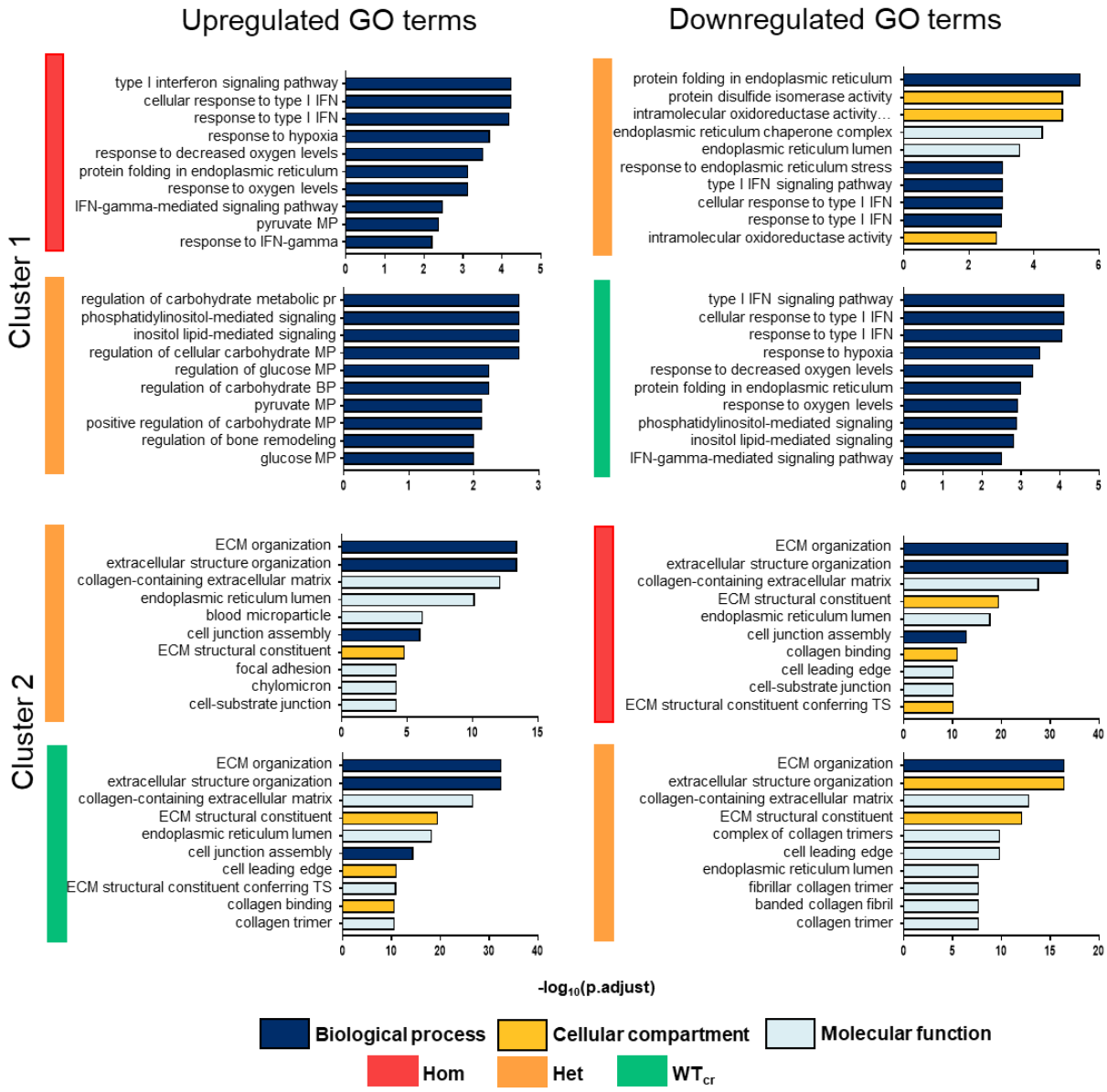
Upregulated GO terms
Downregulated GO terms
Cluster 1
Cluster 2
type I interferon signaling pathway
cellular response to type I IFN
response to type I IFN
response to hypoxia
response to decreased oxygen levels
protein folding in endoplasmic reticulum
response to oxygen levels
IFN-gamma-mediated signaling pathway
pyruvate MP
response to IFN-gamma
protein folding in endoplasmic reticulum
protein disulfide isomerase activity
intramolecular oxidoreductase activity…
endoplasmic reticulum chaperone complex
endoplasmic reticulum lumen
response to endoplasmic reticulum stress
type I IFN signaling pathway
cellular response to type I IFN
response to type I IFN
intramolecular oxidoreductase activity
regulation of carbohydrate metabolic pr
phosphatidylinositol-mediated signaling
inositol lipid-mediated signaling
regulation of cellular carbohydrate MP
regulation of glucose MP
regulation of carbohydrate BP
pyruvate MP
positive regulation of carbohydrate MP
regulation of bone remodeling
glucose MP
type I IFN signaling pathway
cellular response to type I IFN
response to type I IFN
response to hypoxia
response to decreased oxygen levels
protein folding in endoplasmic reticulum
response to oxygen levels
phosphatidylinositol-mediated signaling
inositol lipid-mediated signaling
IFN-gamma-mediated signaling pathway
ECM organization
extracellular structure organization
collagen-containing extracellular matrix
endoplasmic reticulum lumen
blood microparticle
cell junction assembly
ECM structural constituent
focal adhesion
chylomicron
cell-substrate junction
ECM organization
extracellular structure organization
collagen-containing extracellular matrix
ECM structural constituent
endoplasmic reticulum lumen
cell junction assembly
collagen binding
cell leading edge
cell-substrate junction
ECM structural constituent conferring TS
ECM organization
extracellular structure organization
collagen-containing extracellular matrix
ECM structural constituent
endoplasmic reticulum lumen
cell junction assembly
cell leading edge
ECM structural constituent conferring TS
collagen binding
collagen trimer
ECM organization
extracellular structure organization
collagen-containing extracellular matrix
ECM structural constituent
complex of collagen trimers
cell leading edge
endoplasmic reticulum lumen
fibrillar collagen trimer
banded collagen fibril
collagen trimer
-log10(p.adjust)
Biological process
Cellular compartment
Molecular function
Hom
Het
WTcr

Figure S5. Gene ontology (GO) analysis of *CALR*ins5-mutated iPSC-derived MKs. Related to Figure 7.

Gene ontology (GO) analysis based on up- and downregulated genes of cluster-wise analysis for the heat map (Figure 7A) shown in the main text. The top 10 GO terms are shown. GO categories biological process, cellular compartment and molecular functions are depicted in dark blue, yellow, and light blue, respectively. Corresponding genotypes are shown in red, orange and green for MKs with homozygous (Hom) or heterozygous (Het) *CALR*ins5, or WT_{cr} MKs, respectively. BP (biosynthetic process), ECM (extracellular matrix), MP (metabolic process), TS (tensile strength), IFN (interferon).

Figure S6.

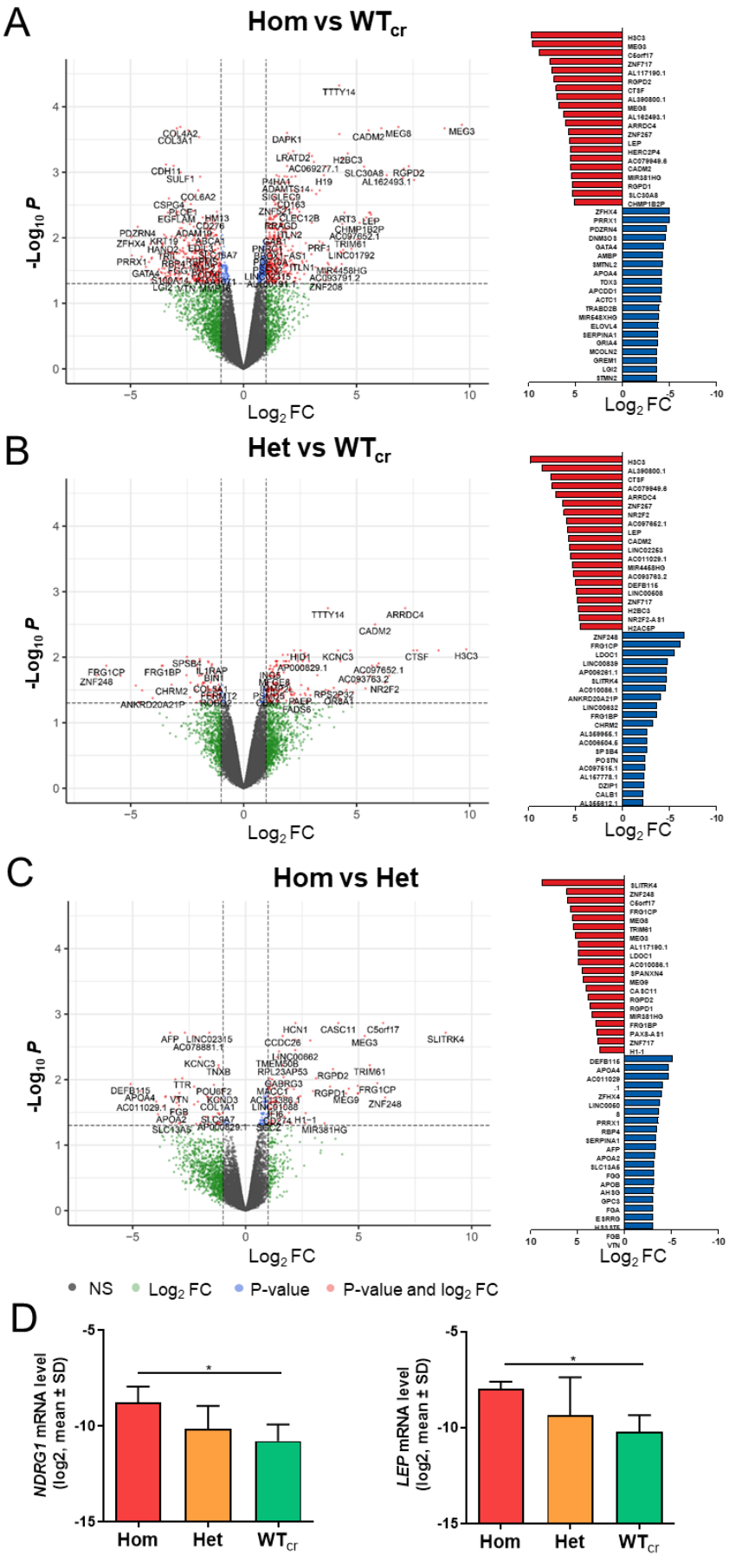
A
Hom vs WTcr
B
Het vs WTcr
C
Hom vs Het
-Log10 P
Log2 FC
NS
Log2 FC
P-value
P-value and log2 FC
D
NDRG1 mRNA level (log2, mean ± SD)
LEP mRNA level (log2, mean ± SD)
Hom
Het
WTcr

Figure S6. Differentially expressed genes (DEGs) in *CALR*ins5-mutated MKs and WT_{cr} MKs. Related to Figure 7.

A., **B.**, and **C**. Volcano plot of differentially expressed genes (DEGs) and list of the top 20 up- and downregulated DEGs among the comparisons: Hom vs WT_{cr} (**A**), Het vs WT_{cr} (**B**), and Hom vs Het (**C**) of CALRins5-muated MKs and control. All genes shown in the list of DEGs are significantly regulated (p≤0.05) Up-and downregulated genes are shown in red and blue, respectively. FC (fold change), Hom (homozygously *CALR*ins5-mutated), Het (heterozygously *CALR*ins5-mutated). **D.** Validation of RNAseq analysis by RT-qPCR for *NDRG1* and leptin (*LEP*) expression. RT-qPCR was performed for two samples also analyzed in RNAseq and one sample from an additional independent differentiation experiment, *n*=3 independent experiments, **p*<0.05. Hom (homozygously *CALR*ins5-mutated), Het (heterozygously *CALR*ins5-mutated).

3. Supplemental Tables

Table S1. Generation of MPN patient-derived CALR iPSCs

Pat.	Diagnosis	CALR mutation	Sample type	Allele burden	iPS clones screened	CALR non-mut clones	CALR Heterozygous clones	CALR homozygous clones
1	pET-MF	ins5	PB	82%	101	0	27	74
2	PMF	del52	PB	51%	64	0	55	9
3	PMF	del31	PB	37%	69	5	64	0

Table S1. iPSCs were generated by reprogramming peripheral blood-derived mononuclear cells from three patients carrying *CALR* del52, ins5, or del31 mutation. Individual colonies were picked and screened for *CALR* genotypes by PCR. Abbreviations: CALR, calreticulin; iPSC, induced pluripotent stem cell; non-mut, non-mutant; PMF, primary myelofibrosis; pET-MF, secondary post essential thrombocythemia myelofibrosis. PB, peripheral blood.

Table S2. CRISPR guide RNAs (gRNAs) to repair homozygous CALR mutations with CRISPR/Cas9. Related to Figure 1.

Mutation	gRNA
*CALR*ins5	5'-AGGCAGAGGACAATTGTCGG -3'
*CALR*del52	5'-ACGAGGAGCAGAGGACAAGG-3'

Table S3. Donor template to repair homozygous CALR mutations with CRISPR/Cas9. Related to Figure 1.

Mutation	Donor Template
*CALR*ins5	5'- GAGGCTTAAGGAGGAGGAAGAAGACAAGAAACGCAAAGAGGAGGA GGAGGCAGAGGACAAGGAGGATGATGAGGACAAAGATGAGGATGA GGAGGATGAGGAGGACAAGGAGGAAGATGA -3'
*CALR*del52	5'- GTGCTCTGCCTGCAGGCAGCAGAGAAACAAATGAAGGACAAACAG GACGAGGAGCAGAGGCTTAAGGAGGAGGAAGAAGACAAGAAACGC AAAGAGGAGGAGGAGGCAGAGGACAAGGAGGATGATGAGGACAAA GATGAGGATGAGGAGGATGAGGAGGACAAGGAGGAAG -3'

Table S4. NGS Data of patient-derived CALR iPSCs and Healthy donor

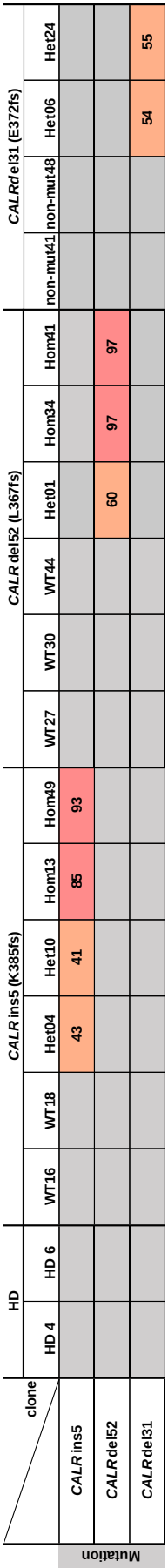

Table S4. Next generation sequencing (NGS) of patient-derived iPSC clones and healthy donors iPSC clones for clinically relevant MPN mutations. In the analyzed gene list (*ABL1, ASXL1, BRAF, BTK, CBL, CSF3R, CXCR4, DNMT3A, ETNK1, EZH2, FLT3, IDH1, IDH2, JAK2, KIT, KRAS, MPL, MYD88, NF-E2, NPM1, NRAS, PTPN11, RUNX1, SETBP1, SF3B1, SH2B3, STAT5B, TET2, TP53, U2AF1, WT1)* no mutation was found. Percentages represent allele frequency (the fraction of mutant reads per total reads) of indicated mutations.

Table S5. List of antibodies used for flow cytometry. Related to Figure 2 and Figure 4.

Antibody	**Company**	**Catalogue number**
APC mouse anti-human CD34	BD, USA	555824
FITC mouse anti-human CD43	BD, USA	555475
PE mouse anti-human CD31	BD, USA	555446
FITC anti-human CD61 clone VI-PL2	BioLegend, USA	336404
Anti-human CD117 (ckit)-PE Cy7 clone 104D2	Thermo Fisher Scientific, USA	25-1178-42
Anti-human CD235a-PE clone HIR2	Thermo Fisher Scientific, USA	12-9987-82
CD45-APC-Vio770 human	Miltenyi Biotec, Germany	130-113-115
APC anti-human CD42b	BioLegend, USA	303912
PE/Cyanina7 anti-human CD41	BioLegend, USA	303718
CD45-APC human	Beckman Coulter. USA	IM2473U
CD15-PC5 human	Beckman Coulter, USA	B49217
MPO-FITC human	Beckman Coulter, USA	IM1874

Table S6. List of primary and secondary antibodies used for Western blot and Immunofluorescence. Related to Figure 1 and Figure 6.

Antibody	**Company**	**Catalogue number**
Monoclonal anti-mutated Calreticulin Rabbit	Dianova, Germany	DIA-CAL-250
Monoclonal anti Calreticulin (D3E6) XP Rabbit #12238	Cell Signaling, USA	12238S
Monoclonal GAPDH (0411): sc-32233 Mouse	Santa Cruz Biotechnology, USA	sc-47724
CD42b Polyclonal Antibody	Thermo Fisher Scientific, USA	PA5-90903
Calreticulin Antibody (1G6A7)	Novus Biologicals, USA	47518SS
Goat anti-rabbit IgG (H+L) Alexa Fluor 555	Thermo Fisher Scientific, USA	A32732
Goat anti-mouse IgG (H+L) Alexa Fluor 647	Thermo Fisher Scientific, USA	A32728

Goat anti-rabbit IgG (H+L) FITC	Thermo Fisher Scientific, USA	F-2765
Goat anti-mouse IgM (H+L) Alexa Fluor 594	Thermo Fisher Scientific, USA	A-11012
Goat anti-mouse Immunoglobulins/HRP, polyclonal	Dako, USA	P0447
Goat anti-rabbit Immunoglobulins/HRP, polyclonal	Dako, USA	P0448

Table S7. List of primers used for qPCR and CALR genotyping PCR. Related to Figure 1, Figure 5 and Figure S1.

Target name		Sequence	Reference
qPCR			
*CALR*del52	Non-.mut allele FRW	CAGGACGAGGAGCAGAGACT	
	Mutant allele FRW	ACAGGACGAGGAGCAGAGAAC	
	Common Rev	GCCTCTCTACAGCTCGTCCTTG	
*CALR*del31	Non-.mut allele FRW	CAAGTCTGGCACCATCTTTG	
	Mutant allele FRW	TCCTCTTTGCGTTTCTTGTC	
	Common Rev	ATCCTCCTTGTCCTCTGTTC	
*CALR*ins5	common FRW	CAAGTCTGGCACCATCTTTG	
	Non-mut allele Rev	TGTCCTCATCATCCTCCTTG	
	mutant Rev	TGTCCTCATCATCCTCCGAC	
ETS1	FRW	TCGATCTCAAGCCGACTCTC	
	REV	CATTCACAGCCCACATCACC	
FLI1	FRW	GTGCTGTTGTCACACCTCAG	
	REV	TACTGATCGTTTGTGCCCCT	
GAPDH	FRW	GTTGAGGTCAATGAAGGGGTC	
	REV	GACCTCAACTACATGGTGAGTTGC	
GATA1	FRW	GGGATCACACTGAGCTTGC	(Szabo et al., 2010)
	REV	ACCCCTGATTCTGGTGTGG	
GFI1B	FRW	AGTTCTGCGGCAAGCGTTTCCA	
	REV	TTTCCGCACACCTGGCACTTGT	
Ki67	FRW	CAGACCCATTTACTTGTGTTGGA	
	REV	ACGCCTGGTTACTATCAAAAGG	
LEP	FRW	CGGTAAGGAGAGTATGCGGG	
	REV	ACCAGAAAGAGTGGAGCCT	
LOX1	FRW	GCATACAGGGCAGATGTCAGA	
	REV	TTGGCATCAAGCAGGTCATAG	
MPL	FRW	CTGCCACTTCAAGTCACGAA	
	REV	CTGCCACTCCAATTCCAGAT	
MPO	FRW	CCGGGATGGTGATCGGTTTT	(Theocharides et al., 2016)
	REV	CAGATGATCCGGGGCAATGA	
MT-ATP6	FRW	CGTACGCCTAACCGCTAACA	
	REV	AGGCGACAGCGATTTCTAGG	
NRDG1	FRW	GACAAAGGCCAAAAGGTCAACA	

	REV	CCATTTCATTGGGAGGGTGGT	
NFE2	FRW	CTGTGACTCCACCACAGGTTT	
	REV	TGAGCAGGGGCAGTAAGTTG	
RUNX1	FRW	CCGAGAACCTCGAAGACATC	
	REV	GTCTGACCCTCATGGCTGT	
vWF	FRW	CAACACCTGCATTTGCCGAA	
	REV	TGACCTGTGACAAGGCACTC	
Genotyping PCR			
*CALR*del52 r	FRW	ACAACTTCCTCATCACCAACG	
*CALR*del31	REV	GGCCTCAGTCCAGCCCTG	
Gentoyping allele specific PCR			
*CALR*ins5	common FRW	TAACTGCAGTGTCAGCGGTG	
	Non-mut allele Rev	TGTCCTCATCATCCTCCTTG	
	mutant Rev	TGTCCTCATCATCCTCCGAC	
PCR for CRISPR-off target products			
CANX	FRW	ACACGTCTTCAGGGTAGGA	
	REV	CAACATCGTAGGGTCTTGGCT	
RABL6	FRW	GCAAAGAGGTACTGGCTACTCC	
	REV	CGGCCTAGAGCTCCTCGTA	
BASP1P1	FRW	GGCGGAGCTAGCACTACAAC	
	REV	GGTGACTTCGGCAGCTTTGG	
IGSF10	FRW	AAGTGAGTGAACCCAGGCAC	
	REV	AGCTTTGGGGAAGGTGATGG	
IGSF5	FRW	TAGAGATTCCTGGTTCCTGGG	
	REV	TCCACCGCCACGTCCTAGATT	
GRIN2B	FRW	TCACCACACACGCTACTTCCAC	
	REV	TTTACAGAGAAGGCTGGCCG	
GLOD5	FRW	CCTTCCATTTGCACTACCTACCT	
	REV	CCCTGGCTAAACTGGGGGAG	
LOC105371816	FRW	TCTTGGAGACAGACTGCTGG	
	REV	GTGTGGGGTCCTGATGCTTTA	

Table S8. Medium composition. Related to Figure 2, Figure 3 and Figure 4.

SFM Medium for "spin-EB" differentiation		
50 %	IMDM	Thermo Fisher Scientific, USA
50 %	Ham's F-12 Nutrient Mixture	Thermo Fisher Scientific, USA
0.5 %	Human Plasbumin 20	Grifols, Germany
2 mM	GlutaMAX	Thermo Fisher Scientific, USA
2 mM	Chemically Defined Lipid Concentrate	Thermo Fisher Scientific, USA
50 µg/ml	L-ascorbic acid	Stemcell Technologies, Canada
6 µg/ml	Transferrin	Merck, Germany
400 µM	1-Thioglycerol	Merck, Germany

EB medium for EB-based differentiation		
	IMDM	Thermo Fisher Scientific, USA
15 %	FBS	Pan Biotech, Germany
1U/ml	Penicillin	Thermo Fisher Scientific, USA
100 mg/ml	Streptomycin	Thermo Fisher Scientific, USA
2 mM	L-Glutamine	Thermo Fisher Scientific, USA
5 %	Protein-Free Hybridoma Medium-II	Thermo Fisher Scientific, USA

0.1 mM	β-mercaptoethanol	Thermo Fisher Scientific, USA
50 µg/ml	L-Ascorbic acid	Sigma Aldrich, Germany
175 µg/ml	hTransferrin	Sigma Aldrich, Germany

Progenitor medium for EB-based differentiation		
	StemPro 34 SFM	Thermo Fisher Scientific, USA
2 mM	L-Glutamine	Thermo Fisher Scientific, USA
1U/ml	Penicillin	Thermo Fisher Scientific, USA
100 mg/ml	Streptomycin	Thermo Fisher Scientific, USA
1X	MEM Non-Essential Amino Acids	Thermo Fisher Scientific, USA

3. Supplemental experimental procedures

Next generation sequencing

For the detection of mutations from gDNA by next generation sequencing (NGS), two panels individually designed and validated for routine hematology diagnostic were used. Either 250ng or 75ng of gDNA were used for library preparation with either a Truseq Custom Amplicon Kit (Illumina, San Diego, USA) or an Ampliseq for Illumina Custom Panel (Illumina) covering the relevant regions of either 31 (*ABL1, ASXL1, BARD1, CALR, CBL, CHEK2, CSF3R, DNMT3A, ETNK1, ETV6, EZH2, IDH1, IDH2, JAK2, KIT, KRAS, MPL, NFE2, NRAS, PDGFRA, PTPN11, RUNX1, SETBP1, SF3A1, SF3B1, SH2B3 (LNK), SRSF2, TCF12, TET2, TP53, U2AF1*)(Kirschner et al., 2018) or 32 genes (*ABL1, ASXL1, BRAF, BTK, CALR, CBL, CSF3R, CXCR4, DNMT3A, ETNK1, EZH2, FLT3, IDH1, IDH2, JAK2, KIT, KRAS, MPL, MYD88, NF-E2, NPM1, NRAS, PTPN11, RUNX1, SETBP1, SF3B1, SH2B3, STAT5B, TET2, TP53, U2AF1, WT1*) associated with hematologic malignancies. The final libraries were sequenced with 2x250bp on a MiSeq (Illumina). The MiSeq onboard software was used (Real time analysis software v1.18.54, Illumina) for demultiplexing and FastQ file generation. Alignment and variant calling were performed with the SeqNext-Module of the SeqPilot-Software (JSI medical systems, Version 4.4.0 Build 509). Variants were called with a bidirectional frequency of >5% (JAK2 V617F and KIT D816V >1%) and reviewed manually.

Cytogenetic analysis

Patient-derived iPSC clones were seeded on matrigel coated 25 cm^2 cell culture flasks. Normal chromosomal constitution was verified by conventional karyotyping of iPSC clones by means of GTG banding at 400 to 550 band level. Metaphase spreads were prepared using standard procedures of blocking cell division at metaphase, hypotonic treatment, and methanol/acetic acid fixation (3:1). The banding techniques included the use of a trypsin pretreatment (GTG-banding) carried out according to standard protocols. Microscopy was performed with Axioplan fluorescence microscope (Carl Zeiss) and IKARUSTM digital imaging systems (MetaSystems, Altlussheim, Germany). An average of 20 mitoses were analyzed for each clone.

Immunofluorescence staining

iPSC colonies were cultured on Matrigel coated coverslips in 4-well-plates. Cells were fixed with 4 % paraformaldehyde (Sigma Aldrich) and blocked with goat serum (Merck Millipore, Darmstadt, Germany). In order to detect the expression of pluripotent markers and mutant CALR, cells were incubated with following primary antibodies at 4 °C overnight: TRA-1-60 (Merck Millipore), OCT3/4 (H-134, Santa Cruz, CA, USA) or mouse monoclonal antibody CAL2 (Dianova, Hamburg, Germany). Cells were washed three times with PBS on the next day and

incubated with corresponding secondary antibodies goat anti-rabbit IgG (H+L) FITC (Thermo Fisher Scientific), goat anti-mouse IgM (H) Alexa Fluor 594 (Thermo Fisher Scientific) or goat anti-mouse IgG Alexa Fluor 647 (for CALR mutant, clone poly4053, BioLegend, San Diego, CA, USA) for 1 h in the dark. Nuclei were stained with DAPI (Vector Laboratories, Burlingame, CA, USA) and coverslips were mounted with Dako Fluorescence Mounting Medium (Dako, Jena, Germany). Fluorescent image analysis was performed using an Axiovert 200 microscope (Carl Zeiss, Jena, Germany) and IPLab Spectrum software (BD, Franklin Lakes, USA).

In order to detect localization of WT and mutand CALR in MKs, cells were fixed with 3,7 % PFA, washed with PBS and permeabilized with 0,1 % Trition-X and 2,5 % BSA. Afterwards cells were incubated with detection reagent for ER-staining and Hoechst (Enzo Life Sciences, Farmingdale,USA) for 20 min at 37°C. Cells were washed with PBS and blocked wit 5 % BSA in PBS. Cells were incubated with the following primary antibodies at 4 °C overnight: polyclonal antibody CD42b (Thermo Fisher Scientific) and mutant CALR antibody (Dianova) or WT CALR monoclonal antibody (Novus, Littleton, USA). On the next day, cells were washed with PBS and incubated with corresponding secondary antibodies goat anti-rabbit IgG Alexa Fluor 555 (H+L) and goat anti-mouse IgG (H+L) Alexa Fluor 647(all Thermo Fisher Scientific) for 1 h at RT. Coverslips were mounted with Fluorescence Mounting Medium (Dako, Carpinteria, USA). Fluorescent image analysis was performed using a confocal Scanning Microscope (LSM 710) microscope and Zeiss 2012 software (both Carl Zeiss, Jena, Germany).

RNA isolation and RT-qPCR

RNA of iPSCs and iPS-cell derived CD34+ HSPCS and CD61+ MKs was isolated using the RNeasy Mini Kit (QIGAEN GmbH, Hilden, Germany) according to manufacturer's protocol. RNA (500 ng) was used for cDNA synthesis. Quantitative RT-qPCR was performed using the 7500 Fast Real-time PCR System (Applied Biosystems by Life technologies, Paisley, UK) with the SYBR Select Master Mix for CFX (Applied Biosystems). The sequences of primers used for-qPCR are listed in Table S7. All primers were purchased from Eurofins-MWG biotech (Ebersberg, Germany). The mRNA expression level of the target gene is determined in % of *GAPDH* or *MT-ATP6*.

SDS-page and Western blot

SDS-Page and Western blot analysis were conducted as previously described (Han et al., 2016). Primary and secondary antibodies are listed in Table S6.

Undirected hematopoietic differentiation of iPSCs into hematopoietic progenitors and myeloid subsets with the "EB-based" protocol

iPSCs were cultured on irradiated mouse embryonic fibroblast feeder layer in KnockOut-DMEM based iPSC medium. More detailed information regarding cell culture conditions can be found in Table S8.

For the generation of iPSC-derived CD34+ HSPCs, CALR iPSCs were subjected to mesoderm commitment and hematopoietic differentiation with an embryonic body (EB)-based protocol modified from the differentiation method described by Kovarova and colleagues (Kovarova and Koller, 2012). CD34+ HSPCs were cultured and differentiated into myeloid subsets in the StemPro 34 SFM medium (Thermo Fisher Scientific) based progenitor medium at the maximum density of $1x10^6$ cells/ml. Details of EB and HSPCs differentiation media are provided in Table S8.

Differentiation of iPSCs into hematopoietic stem cells and myeloid subsets with the "spin-EB" protocol

Feeder-free iPSC culture was maintained on matrigel coated 6-well plates and routinely passaged with 1 ml accutase or 0.5 mM EDTA (Thermo Fisher Scientific). To enhance single cell survival, 10 µM ROCK inhibitor Y-27632 was added to the maintenance culture medium StemMACs iPS Brew XF for 24 h after seeding. iPSC medium was changed daily.

Human iPSCs were differentiated into HSPCs, MKs and erythrocytic cells adapted from the differentiation protocol by Liu et. al (Liu et al., 2015). Briefly, iPSCs were seeded into U-bottom-shaped 96-well plates with a density of 3,000 cells/well in cytokine supplemented serum-free medium (SFM). To allow spheroid formation, plates were spun at 380 g for 5 min. From day 2 to day 8, cells were cultured in SFM with 10 ng/ml VEGF (Miltenyi Biotec), 10 ng/ml BMP4 (Miltenyi Biotec), 10 ng/ml bFGF (Peprotech, Hamburg, Germany) and SCF (0.5 % supernatant of SCF secreting CHO KLS cells). From day 8 onwards, BMP4 and VEGF were removed from the medium. On day 11, 20 ng/ml TPO (Miltenyi Biotec) was added to the medium. On day 14, cells were harvested and filtered through a 100 µm filter to separate the EBs from the suspension cells. Single cells were analyzed by flow cytometry and purified for CD61+ and CD34+ cell fractions. More detailed information on SFM Medium is given in Table S8.

Cell morphology analysis

Phase contrast images of iPSC generation and differentiation were obtained with EVOS FL microscope (Thermo Fisher Scientific). To characterize the morphologies of iPSC-derived precursors and myeloid subsets, cells were spun onto slides with Shandon Cytospin 4

cytocentrifuge (Thermo Fisher Scientific) and stained with Diff Quik solution 1 and 2 (Medion Diagnostics, Düdingen, Switzerland) after methanol fixation. Images were acquired using a Leica DMRX microscope and Leica Application Suite software (Leica Microsystems).

MPO cytochemical staining

In order to evaluate MPO functional activity, iPSC-derived hematopoietic cells at differentiation day 15 were centrifuged onto slides and fixed with LEUCOGNOST® Fixing Mixture. The fixed cells were stained with LEUCOGNOST® POX Kit according to the manufacturer's instructions. Counterstaining of nucleus was performed using Mayer's hemalum solution and slides were mounted with Kaiser's glycerol gelatin (the Kit and all reagents were obtained from Merck Millipore). Images were acquired as described above.

Flow cytometry analysis

To evaluate cell surface progenitor and lineage specific markers, single cells were analyzed on day 10, day 12 and day 14 of "spin-EB" differentiation and on day 10 and day 15 of "EB-based" differentiation. Cells were harvested and passed through a 100 µm cell strainer, centrifuged at 350 g for 5 min. After washing with ice cold FACS buffer, single cells were incubated with lineage-specific antibodies at 4°C for 30 min. Stained cells were resuspended in 300 µl FACS buffer and analyzed on a FACS Canto II (BD). All staining and washing steps were performed in FACS buffer consistent of PBS supplemented with 2 mM EDTA and 2 % BSA (PAN Biotech, Aidenbach, Germany).

To identify the intracellular MPO expression, differentiated hematopoietic cells at day 15 of "EB-based" differentiation were fixed and permeabilized using Fix & Perm Cell Permeabilization Kit (Thermo Fisher Scientific). Cells were firstly stained for cell surface markers CD15 and CD45 for 20 min at room temperature (RT), followed by intracellular MPO staining for 20 min at RT after fixation and permeabilization. Stained cells were evaluated by Gallios flow cytometer (Beckman Coulter, Krefeld, Germany). All data were analyzed by FlowJo™ (version 10, Oregon, USA).

Full list of antibodies is summarized in Table S5. In each experiment matched Ig isotype controls were used to set background fluorescence.

CRISPR/Cas9-mediated repair of homozygous *CALRins5* and *CALRdel52* mutation in iPSCs

The Alt-R™ CRISPR-Cas system (Integrated DNA Technologies IDT, Coralville, USA) was used to efficiently correct homozygous *CALRins5* or *CALRdel52* mutations in MPN patient-specific iPSCs. For precise editing the Alt-R® S.p HiFi Cas9 Nuclease V3 was used together with a single-stranded donor template to repair the double strand break by the cellular

repair mechanisms of homology directed repair (HDR). In brief, guide RNA composing of crRNA and tracrRNA was combined with HiFi. Cas9 Nuclease to assembly the CRISPR-Cas9 ribonucleoprotein complex. Singularized iPSCs were gently mixed with the ribonucleoprotein complex, single-stranded donor template, and electroporation enhancer. Nucleofection was performed using the 4D NucleofectorTM X-Unit and the P3 Primary Cell 4D-NucleofectorTM X, Kit S (both from Lonza, Basel, Switzerland). HDR was stimulated by HDR enhancer (IDT, Coralville, USA). After nucleofection, iPSCs were seeded on previously coated Laminin 521 (Biolamina, Sundbyberg, Sweden) plates to support cell viability in StemMACS™ iPS-Brew XF (Miltenyi Biotec, Bergisch Gladbach, Germany) supplemented with 10 µM of Rock inhibitor Y-27632 and 1x CloneR (Stemcell Technologies). Repair of *CALR*ins5 and *CALR*del52 mutation was verified by allele-specific or flanking PCR, respectively, and proofed by Sanger sequencing and Western blot. Possible off-target effects were excluded by PCR reaction of off-target sites and subsequent Sanger sequencing. Sequences of crRNA, donor template and primers are provided in Table S2 and 3.

Purification of CD34+ HSPCs and CD61+ megakaryocytes by magnetic activated cell sorting

On day 25-35 of "EB-based" differentiation and on day 14 of "spin-EB" differentiation anti-CD34 and anti-CD61 MicroBeads (Miltenyi Biotec, Bergisch Gladbach, Germany) were used to separate HSPCs and MKS, respectively. Purification of cells was performed according to the protocol provided by the manufacturer. In brief, single cell suspension was incubated with CD61 or CD34 MicroBeads for 15 or 30 min, respectively, to label the cells magnetically. Cell suspension was loaded onto a LS column installed in a magnetic field. After washing three times with MACS buffer consisting of PBS supplemented with 5 % FCS (Thermo Fisher Scientic) and 2 mM EDTA to remove unbounded cells, the column was removed from the magnetic field and positively selected cell fraction was eluted with 5 ml of MACS buffer from the column. After centrifugation at 300 g for 10 min, purified cells were counted and further processed. CD61+ MKs and CD34+ HSPCs were either snap frozen for RT-qPCR or used for transmission electron microscopcy or seeded in Colony-Forming Unit Assay, respectively.

Colony-forming unit assay of CD34+ HSPCs

Purified CD34+ cells were seeded in MethoCult^{TM} (Stemcell Technologies) supplemented with 20 ml IMDM (Thermo Fisher Scientific), 50 ng/ml hSCF, 10 ng/ml hIL-3. 10 ng/ml hGMSCF and 14 ng/ml hEPO (all ImmunoTools Friesoythe; Germany) in a cell density of 5,000 cells/ml. After 10-12 days of culture at 37° C, colonies were identified and counted based on morphology using light microscopy (Motic, Barcelona, Spain).

Transmission electron microscopy

iPSC-derives CD61+ megakaryocytes at day 14 of “spin-EB” differentiation were prepared as described previously. Purified MKs were washed with PBS and fixed with 3 % glutaraldehyde for at least 2 h at RT, followed by embedding in 5 % low melting agarose (Merck). Gelatinated blocks were washed in 0.1 M Soerensen’s phosphate buffer (Merck) and post-fixed in 17 % sucrose buffer (Merck) containing 1 % OsO4 (Roth, Karlsruhe, Germany). Subsequently, specimens were dehydrated performing an ascending ethanol series repeating the last step for three times (30, 50, 70, 90, and 100 % ethanol; 10 min each step). Dehydrated samples were consecutively incubated in propylene oxide (Serva, Heidelberg Germany) for 30 min, in a mixture of EPON resin (Serva) and propylene oxide (1:1) for 1 h, and in pure EPON for 1 h. EPON polymerization was conducted at 90 °C for 2 h. Ultrathin sections of 70−100 nm were cut with a Reichert Ultracut S ultramicrotome (Leica, Wetzlar, Germany) equipped with a diamond knife (Leica) and picked up on copper−rhodium grids (Plano, Wetzlar, Germany). Contrast was enhanced by staining with 0.5 % uranyl acetate and 1 % lead citrate (both EMS, Munich, Germany). Samples were viewed at an acceleration voltage of 60 kV using a Zeiss Leo 906 (Carl Zeiss, Jena, Germany) transmission electron microscope. Image processing and analysis was performed using ImageJ (Schneider et al., 2012).

Preparation of samples for RNA Sequencing

RNA of purified CD61+ MKs was isolated as described in Supplementary Information. Quality was verified by TapeStation 4200 (Agilent, Santa Clara, USA) to determine RNA integrity number (RIN). RNA concentration was measured with Fluorometer Quantus™ (Promega, Fitchburg, USA). According to manufacturer’s protocol, ribosomal RNA was depleted using NeBNext® rRNA Depletion Kit, prior to library preparation with NeBNext®Ultra™II Directional RNA Library Prep Kit for Illumina (both New England BioLabs, Ipswich, USA) using an RNA input of 100 ng per sample (New England BioLabs, Ipswich, USA). Subsequently, samples were sequenced in paired end reads (2x76 bp, dual indexed) on two NextSeq High Output Kits v2.5 (150 cycles) on a NextSeq 500 instrument (both Illumina, San Diego, USA) to have sufficient reads for data analysis.

4. References

Han, L., Schubert, C., Köhler, J., Schemionek, M., Isfort, S., Brümmendorf, T.H., Koschmieder, S., and Chatain, N. (2016). Calreticulin-mutant proteins induce megakaryocytic signaling to transform hematopoietic cells and undergo accelerated degradation and Golgi-mediated secretion. J. Hematol. Oncol. *9*, 1–14.

Kirschner, M., Maurer, A., Wlodarski, M.W., Ventura Ferreira, M.S., Bouillon, A.-S., Halfmeyer, I., Blau, W., Kreuter, M., Rosewich, M., Corbacioglu, S., et al. (2018). Recurrent somatic mutations are rare in patients with cryptic dyskeratosis congenita. Leukemia *32*, 1762–1767.

Kovarova, M., and Koller, B. (2012). Differentiation of mast cells from embryonic stem cells. Curr. Protoc. Immunol.

Liu, Y., Wang, Y., Gao, Y., Forbes, J.A., Qayyum, R., Becker, L., Cheng, L., and Wang, Z.Z. (2015). Efficient Generation of Megakaryocytes From Human Induced Pluripotent Stem Cells Using Food and Drug Administration-Approved Pharmacological Reagents. Stem Cells Transl. Med. *4*, 309–319.

Schneider, C.A., Rasband, W.S., and Eliceiri, K.W. (2012). NIH Image to ImageJ: 25 years of image analysis. Nat. Methods *9*, 671–675.

Szabo, E., Rampalli, S., Risueño, R.M., Schnerch, A., Mitchell, R., Fiebig-Comyn, A., Levadoux-Martin, M., and Bhatia, M. (2010). Direct conversion of human fibroblasts to multilineage blood progenitors. Nature *468*, 521–526.

Theocharides, A.P.A., Lundberg, P., Lakkaraju, A.K.K., Lysenko, V., Myburgh, R., Aguzzi, A., Skoda, R.C., and Manz, M.G. (2016). Homozygous calreticulin mutations in patients with myelofibrosis lead to acquired myeloperoxidase deficiency. Blood *127*, 3253–3259.